Ph.D. DISSERTATION

System Design of Advanced Multi-Beam and Multi-Range Automotive Radar

다중빔 다중범위 차량용 레이더 시스템 설계

BY

JAE-EUN LEE

FEBURARY 2017

DEPARTMENT OF ELECTRICAL AND
COMPUTER ENGINEERING
COLLEGE OF ENGINEERING
SEOUL NATIONAL UNIVERSITY

Ph.D. DISSERTATION

System Design of Advanced Multi-Beam and Multi-Range Automotive Radar

다중빔 다중범위 차량용 레이더 시스템 설계

BY

JAE-EUN LEE

FEBURARY 2017

DEPARTMENT OF ELECTRICAL AND
COMPUTER ENGINEERING
COLLEGE OF ENGINEERING
SEOUL NATIONAL UNIVERSITY

System Design of Advanced Multi-Beam and Multi-Range Automotive Radar

다중빔 다중범위 차량용 레이더 시스템 설계

지도교수 김 성 철
이 논문을 공학박사 학위논문으로 제출함

2017년 2월

서울대학교 대학원

전기 컴퓨터 공학부

이 재 은

이재은의 공학박사 학위 논문을 인준함

2017년 2월

위 원 장: _____
부위원장: _____
위 원: _____
위 원: _____
위 원: _____

Abstract

As the number of vehicles on the road is increased, the incidence of traffic accident is gradually increased and the number of death on roads is also increased. Most accidents are due to carelessness of the driver. If the vehicle can actively recognize the dangerous situation and alert the driver to avoid accident, it will be a great help to the driver. As concern for safety and driver assistance increases, needs for driver assistance system (DAS) are consistently increasing. Moreover, with the grooming demand for autonomous driving, there has been paid a great attention to the incorporation of multiple sensors. Various sensors for safety and convenience are being introduced for automobiles. The detection performance of the automotive radar looks outstanding compared to other sensors such as Lidar, camera, and ultrasonic sensors, in poor weather conditions or environmental conditions of the roads. Among many applications using automotive radars, the adaptive cruise control (ACC) and the autonomous emergency braking (AEB) using forward looking radars are the most basic functions for safety and convenience. Using ACC and AEB functions, drivers can be guaranteed safety as well as convenience when visibility is poor under bad weather conditions.

Generally, the radar system for ACC and AEB had been composed of singe long-range radar (LRR) and two of short-range radar (SRR) and the system cost was very expensive. However, the cost can be lowered by the concept of multi-beam, multi-range (MBMR) radar which consist of integrated narrow long range beam and wide short range beam in a single radar sensor.

In this dissertation, we propose an advanced MBMR radar for ACC and AEB using 77 GHz band and highly integrated RF ICs. The detection specifications are investi-

gated base on theoretical radar principles and effective design concepts are suggested to satisfy the specifications. We implemented an actually working forward looking MBMR radar and performed experiments to verify the detection performance.

To overcome the limitation of radar hardware resources for cost-effective design, we propose novel signal processing schemes to recognize environment on roads which are regarded as impossible with automotive radar. Characteristics of an iron tunnel which deteriorate the detection performance of the radar are analyzed and a measure for the recognition is proposed.

Moreover, the recognition method is expanded to harmonic clutters which are caused by man-made structures on roads containing periodic structures such as iron tunnels, guardrails, and sound-proof wall. The harmonic clutter suppression method is also proposed to enhance the quality of the received signal and improve the detection performance of the radar.

All experiments are performed using the proposed MBMR radar to verify the detection performance and the usefulness of proposed signal processing methods for recognition and suppression of clutters on roads.

keywords: Automotive Radar, Clutter Recognition, Clutter Suppression, Multi-Beam, Multi-range, MBMR

student number: 2013-30251

Contents

Abstract i

Contents iii

List of Tables vi

List of Figures vii

1 Introduction 1

2 A Multi-Beam and Multi-Range FMCW Radar using 77 GHz Frequency Band for ACC and AEB 6

2.1 Introduction 6

2.2 System Design of Advanced MBMR Radar 7

2.3 Waveform and Signal Processing Structure Design 14

2.4 Advanced Singal Processing Technique for AEB 19

2.5 Design Results 20

2.6 Experimental Results 22

2.6.1 Anechoic Chamber 22

2.6.2 Field Test 27

2.7 Summary 29

3 Iron-tunnel Recognition **30**

3.1 Introduction 30

3.2 Iron-Tunnel Recognition 32

3.2.1 Radar Model 32

3.2.2 Spectral Characteristics of an Iron-Tunnel 34

3.2.3 Measuring Spectrum Spreading 40

3.3 Experimental Result 45

3.3.1 Iron-Tunnel Recognition 45

3.3.2 Early Target Detection and Prevention of Target Drop 49

3.4 Summary 53

4 Clutter Suppression **55**

4.1 Introduction 55

4.2 Clutter Recognition 57

4.2.1 Radar Model 57

4.2.2 Spectral Analysis of Road Environment 62

4.2.3 Proposed Clutter-recognition Method (Measuring Harmonics of Clutter) 64

4.3 Clutter Suppression 69

4.3.1 Proposed clutter suppression method 69

4.3.2 Verification using real data 71

4.4 Experimental results 74

4.5 Summary 81

5 Conclusion and Future Works **82**

Abstract (In Korean) **89**

List of Tables

2.1 System requirements of MBMR radar 12

2.2 System parameters of MBMR radar 13

3.1 Iron-tunnel profile 42

3.2 Spectrum speading and profile of various tunnels 46

4.1 Profile of various harmonic clutters and the level of harmonic clutter . 73

List of Figures

2.1 Radar system architecture of an MBMR radar. 11

2.2 Waveform and time diagram of transmitting signal. 16

2.3 Signal processing architecture of an FMCW radar. 18

2.4 Waveform and time diagram of transmitting signal for AEB. 20

2.5 Design result of RF PCB board. 21

2.6 Measurement of radiation pattern of TX#1 antenna. 23

2.7 Measurement of radiation pattern of TX#2 antenna. 24

2.8 RF anechoic chamber with target simulator. 25

2.9 Measurement result of angular power spectrum. 26

2.10 Test vehicle installed MBMR radar. 27

2.11 Test scenario and result of the detection coverage performance. 28

3.1 Radar system architecture. 34

3.2 Spectrogram of the received radar signal under various road conditions. 39

3.3 Spectrogram and spectral spreading. 44

3.4 Iron-tunnel recognition using the proposed spectral spreading measure (t_0:tunnel entry time, t_r:tunnel recognition time). 48

3.5 Iron-tunnel recognition time according to the recognition threshold . . 49

3.6 Comparison of detection result (Early detection) (tunnel entry time, $t_0 = 15.75s$, tunnel recognition time, $t_r = 13.25s$) 51
3.7 Comparison of detection result (Early detection) (tunnel entry time, $t_0 = 12.00s$, tunnel recognition time, $t_r = 8.25s$) 52

4.1 Spectrograms and harmonograms of the received radar signal under various road conditions. 61
4.2 Analysis of the level of harmonic clutter under various road conditions. 68
4.3 An example of clutter suppression results in an iron tunnel. 72
4.4 Results of harmonic clutter suppression. 77
4.5 Comparison of detection result (Early detection). 79

Chapter 1

Introduction

According to the report of World Health Organization, more than 1.2 million people die each year on the roads and road traffic crashes are a leading cause of death among young people [1]. Among various types of traffic accidents, over 90% of accidents are caused by human errors. As concern for safety and driver assistance increases, needs for driver assistance system (DAS) are consistently increasing. Moreover, with the grooming demand for autonomous driving, there has been paid a great attention to the incorporation of multiple sensors [2], [3]. Various sensors for safety and convenience are being introduced for automobiles. The detection performance of the automotive radar looks outstanding compared to other sensors in poor weather conditions or poor environmental conditions of the roads.

There are a lot of DAS applications using automotive radar such as adaptive cruise control (ACC), autonomous emergency braking (AEB), blind spot detection (BSD), cross traffic alert (CTA), and rear cross traffic alert (RCTA) system. ACC system adjust the velocity of the own vehicle to the distance and velocity of the target vehicle in front using forward looking radar which detect the target information such as range,

velocity, and angle. The vehicles on adjacent lanes can be detected by BSD system which is mounted in the both corners of the rear bumper. A visible or an audible warning for drivers from BSD sensor would be helpful in a dangerous lane changing situation. Generally, 24 GHz radar is used as a BSD sensor. CTA system can prevent accidents due to the unrecognized crossing traffic at the intersection detecting crossing vehicles in invisible region using frontal corner radars. RCTA system can assist drivers in backing up by warning using rear corner radars detecting approaching vehicles or pedestrians.

Among many applications of the automotive radar, the adaptive cruise control (ACC) and the autonomous emergency braking (AEB) using forward looking radars are the most basic functions for safety and convenience [4]–[6]. Using ACC and AEB functions, drivers can be guaranteed safety as well as convenience when visibility is poor under bad weather conditions.

Generally, the radar system for ACC and AEB had been composed of singe long-range radar (LRR) and two of short-range radar (SRR), however, most of forward looking radars are multi-beam, multi-range (MBMR) radars which consist of integrated narrow long range beam and wide short range beam in a single radar sensor [7]. The installation rate of automotive radar worldwide will increase because of its low cost and small size by employing MBMR radar.

In this dissertation, we propose an advanced MBMR radar for ACC and AEB using 77 GHz band and highly integrated RF ICs. The detection specifications are investigated base on theoretical radar principles and effective design concepts are suggested. We implemented an actually working forward looking MBMR radar and performed experiments to verify the detection performance.

As the signal quality of automotive radars decreases by downsizing, their detec-

tion performance should be maintained for the safety. Moreover, their detection performance can be deteriorated by man-made structures on roads such as iron tunnels, guardrails, or soundproof walls that have high reflectivity for electromagnetic waves and generate harmonic clutters which are due to periodic structures on roads. There have been several studies about reflection or diffraction on road surfaces [8]–[10]. These studies have found that the detection performance of radar is dependent on the surface roughness and road slopes. Meanwhile, there have been few studies on clutters caused by man-made structure on roads [11], [12]. These studies focused on ultra wideband pulse radars, so their application to frequency-modulated continuous waves (FMCW) [13]–[15] is not appropriate. In addition, there have been several approaches to discriminate over-head or neighboring structures from stationary targets on roads [16]–[18]. However, few of them considered the suppression method to improve the detection performance of radar despite of clutters on roads.

To overcome the limitation of radar hardware, we need to implement signal-processing techniques to improve the detection performance. Novel signal processing algorithms for the recognition and suppression of clutter signals from environments on roads to as a value added function. Clutter signal from densely distributed man-made structures can deteriorate the detection performance of the radar. We propose an iron-tunnel recognition scheme which affect severely on the detection performance. The effect of the proposed method is verified by the field test using the proposed MBMR radar. To expand the recognition of road environments, we investigate the spectral and harmonic analysis. Many clutter signal indicate the harmonic characteristics due to the periodic structures. We propose a recognition method of harmonic clutters and suppression method to improve the quality of received signal.

The remainder of this dissertation is organized as follows. In Chapter 2, system

design of the MBMR radar using FMCW modulation is presented. In the section 2.2 of Chapter 2, the fundamental radar equation is analyzed, the required specification is introduced, design of system parameters, such as bandwidth, chirp duration, and sampling rate, is explained, and the detection resolution in terms of range, velocity, and angle is calculated. To satisfy the specification and the detection performance, the harware design including antenna type, antenna spacing, the number of antenna, and arrangement of active and passive circuits is proposed. In the section 2.3 of Chapter 2, the designs of waveform and signal processing structure for MBMR are also proposed to have effective detection performance for both LRR and SRR introducing basic principles of FMCW radar. In the section 2.4 of Chapter 2, the design results are presented with implemented RF PCB and measurement of the radiation pattern. The experimental results of the detection performance satisfying detection-range coverage are presented in the section 2.5 of Chapter 2.

In Chapter 3, we propose a novel iron-tunnel recognition method to overcome the deterioration in the target or vehicle detection performance due to iron tunnel clutters. The proposed method recognizes an iron tunnel by analyzing the spectrum characteristics of the received radar signal under different road conditions. We observed that an iron tunnel causes a high intensity scattering over a wide frequency band. Thus, the proposed method measures the degree of spectral spreading by incorporating the entropy concept. The experimental data used in this paper are obtained from a 77-GHz forward-looking FMCW radar for ACC. We demonstrate that the proposed method can successfully detect iron tunnel. In addition, the results show that the missing problem of a target vehicle in an iron tunnel under ACC using radar is improved by overcoming the deterioration in the detection performance around or inside iron tunnels. In Section 3.2 of Chapter 3, the description of the radar model used in the research and the anal-

ysis of the spectral characteristics of the received signal in accordance with various road environments are explained. Then, the proposed method is presented in detail. In Section 3.3 of Chapter 3, the experimental results of recognizing an iron tunnel as well as the results that show the improvement in the ACC performance are provided.

In Chapter 4, we propose a novel harmonic clutter recognition and suppression method to overcome the deterioration of detection performance due to harmonic clutters. The proposed method recognizes harmonic clutters by analyzing the spectrum of the received signal under different road conditions. We observed that the spectrum contains equally spaced frequency peaks which are harmonic clutters due to periodic structures such as iron tunnels, guardrails, and sound-proof walls. The proposed recognition method measures the level of clutter by applying the discrete Fourier transform (DFT) to the spectrum in frequency domain and incorporating the concept of the peak-to-average-power ratio (PAPR). The proposed suppression method restrains harmonic clutters by reducing the level of clutter. Raw experimental data were obtained using a 77-GHz forward-looking FMCW radar for the ACC and AEB. We demonstrate that the proposed method can successfully recognize and suppress harmonic clutters using real field data. In addition, the detection results show that the problem of the late detection of a target vehicle in an iron tunnel under ACC is improved by using the proposed clutter-suppression method. In Section 4.2 of Chapter 4, we present a description of the radar model and the spectral analysis of the received signal in accordance with various road environments. Then, we discuss in detail the proposed harmonic clutter-recognition method. In Section 4.3 of Chapter 4, we present and verify the proposed suppression method by performing the software-in-the-loop (SIL) test using real data obtained from the radar. In Section 4.4 of Chapter 4, we show the experimental results of the improved early detection in the ACC performance.

Chapter 2

A Multi-Beam and Multi-Range FMCW Radar using 77 GHz Frequency Band for ACC and AEB

2.1 Introduction

As the importance of safety increases, various sensors for safety are applied to automobiles. The installation rate of forward looking automotive radar is expected to increase enormously because the autonomous emergency braking (AEB) system has appointed as a regulation in the EU and the U.S. [19]. The adaptive cruise control (ACC) can be also widely used for the safety and convenience [6] with the grooming demand for autonomous driving. Conventional radar system has single-beam area [20], [21], however, the demands for smaller size and lower cost encouraged the development of a multi-beam and multi-range (MBMR) radar [7]. The cutting-edge technology of highly integrated RF ICs accelerated the development of an MBMR radar. The angular resolution of 77 GHz radar is 3 times better than that of 24 GHz radar with same antenna aperture size. The range resolution is also better because of permitted frequency band is 5 times wider in 77 GHz band up to 1 GHz whereas 200 MHz in 24 GHz

band due to ISM band limitation. The demand for high performance MBMR radar is increasing to satisfy detection requirements as a cost-effective solution.

In this chapter, we propose an advanced MBMR radar using 77 GHz frequency band for ACC and AEB. The proposed MBMR radar consist of narrow beam for long range detection and wide beam for short range detection with advanced detection performance. The design concept for cost-effective MBMR radar is presented considering the detection performance. The RF hardware was highly integrated including antennas, RF active circuits, and RF passive circuits. The design of FMCW waveform and signal processing is introduced to extract target information, effectively, from the received signal. We demonstrate the results of implementation and measurement in RF anechoic chamber using the proposed MBMR radar. In addition, the detection results show that the detection performance of the proposed MBMR radar.

This chapter is organized as follows, In Section 2.2, we introduce a design concept of the advanced MBMR radar considering the requirement of the detection performance. In Section 2.3, we show the signal processing structures for the extraction of target information. The design and measurement results are demonstated in Section 2.4 and the experiments to verify the detection performance of the proposed MBMR radar are illustrated though the real data using the proposed MBMR radar in Section 2.5. We summarize and conclude this chapter in Section 2.6.

2.2 System Design of Advanced MBMR Radar

In this section, an advanced MBMR radar using 77 GHz frequency band and SiGe RF ICs is presented. The proposed MBMR radar has advanced detection performance in the aspect of detection range and target discrimination as well as smaller size compared

with previous 24 GHz MBMR radar because the wavelength is shorter.

A forward looking MBMR radar need to detect long range with narrow beam area and short range with wide beam area simultaneously with limited frequency resources and transmit power. The system requirements of 77 GHz forward looking radar for ACC and AEB function are listed in Table 2.1. The frequency range is 76 GHz to 77GHz and the transmit power limitation is $10mW$. Generally, cycle time of radar operation is less than $100ms$ due to sufficient detection of targets for the safe control of the vehicle. The maximum detection range is farther than $200m$ and $60m$ for long range area and short range area, respectively. The detectable relative velocity range is from $-180kph$ to $+180kph$ where the negative velocity means the on-coming. The ACC function operate up to $180kph$ of own vehicle speed. The field of view is up to 20 degree and 60 degree, respectively. The radar equation should be considered preferentially to determine the maximum detection target range theoretically satisfying given requirements. The radar equation is a basic theory for design of radar system which is defined as follows,

$$P_r = \frac{P_t G_t}{4\pi R^2} \frac{\sigma}{4\pi R^2} A_e \tag{2.1}$$

where P_r is the received signal power, P_t is the output power of the transmitted signal, G_t is the gain of the TX antenna, σ is the Radar Cross Section (RCS) of a target, R is the distance of a target, and A_e is the effective area of receiving antenna. The first term is the power density of the transmitted signal from the directive antenna with certain antenna beam pattern, the second term is the power density of the received signal which is reflected from the target with RCS (σ), and the received power density from the reflected signal is gathered through the antenna aperture of the receiving antenna.

The maximum detectable range can be calculated using Eq.(2.1) as follows

$$R_{max} = \sqrt[4]{\frac{P_t G_t \sigma A_e}{(4\pi)^2 P_{min}}} = \sqrt[4]{\frac{P_t G_t G_r \lambda^2}{(4\pi)^3 P_{min}}} \tag{2.2}$$

where G_r is the gain of the RX antenna, λ is the wavelength, and P_{min} is the minimum detectable power of the received signal.The minimum detectable power depends on receiver noise bandwidth (B_n), noise figure (F), temperature (T), and required minimum signal-to-noise ration (SNR).

$$P_{min} = kTB_nF(SNR)_{min} \tag{2.3}$$

where k is the Boltzmann's constant (J/K). A receiver with narrow noise bandwidth is more sensitive than a receiver with wider noise bandwith. Noise figure is a measure of how much noise the receiver contributes to a signal. Increasing temperature affects receiver sensitivity by increasing input noise. We can obtain more practical radar equation when we consider the SNR including losses such as propagation losses, losses due to the radome and RF components, and processing losses in the noise term. In order to satisfy the system requirements, an MBMR radar with dual transmitter (TX) channel and 12 receiver (RX) channel is proposed as shown in Figure 2.1. The TX port #1 for long range with narrow beam is connected to multiple Series-Fed Patch Antenna (SFPA). The TX port #2 for short range with wide beam is connected to a single array to have wide angle coverage upto 90 degree. The proposed SFPA have a lot of advantages, such as a compact line length feed network [22], light weight, and simple structure. To avoid mutual interference from other radar sensors at the front, traveling wave excitation with slant polarization of 45° is applied. Because the received signal power from direct transmission at the front is greater than other reflected signals among various situation of interference on the road, the prevention of direct transmission is very important for the stable operation of the radar. The TX RF IC contains

phase locked loop (PLL) with low noise performance, voltage controlled oscillator (VCO), and splitter with distributes the output of the VCO to each TX ports and local oscillator (LO) port to the RX RF ICs. The output of TX can be controlled by the amplifier which operate as an amplifier and switch to control the transmission. The output port of LO is divided by the power divider to each RX RF ICs. Each of the RX RF IC is comprised of 4 channel low noise amplifier (LNA), mixer and connected to the Analog-to-Digital Converter (ADC) through band-pass filter (BPF) to filter the direct current (DC) noise due to the direct conversion and high frequency harmonics from the mixer. The bandwidth of the BPF is designated by the maximum beat frequency corresponded to the maximum detection range and Doppler frequency by the relative speed. Three RX RF ICs are used to implement 8 receiving channel for long range and 4 channels for short range. Each channel of RX port #1 is connected to triple-SFPA as uniform linear array (ULA) with 1.8λ spacing and RX port #2 is connected to a single array with 0.6λ spacing. Rx antennas are also applied slant polarization of 45° to mitigate transmitted signals at the front. Received signals from each channel are processed by digital signal processor (DSP) to extract informations from targets. Generally, the layer of antenna and RF ICs are separated to avoid the mutual interference between RF components, however, the proposed architecture integrated antenna, RF ICs, and RF passive circuits on the same RF PCB layer. The size and the cost of the proposed radar can be reduced through the hardware structure. To prevent the mutual i between antennas and RC ICs, a metallic cavity specially designed for shielding RF signals is covered on RF circuits.

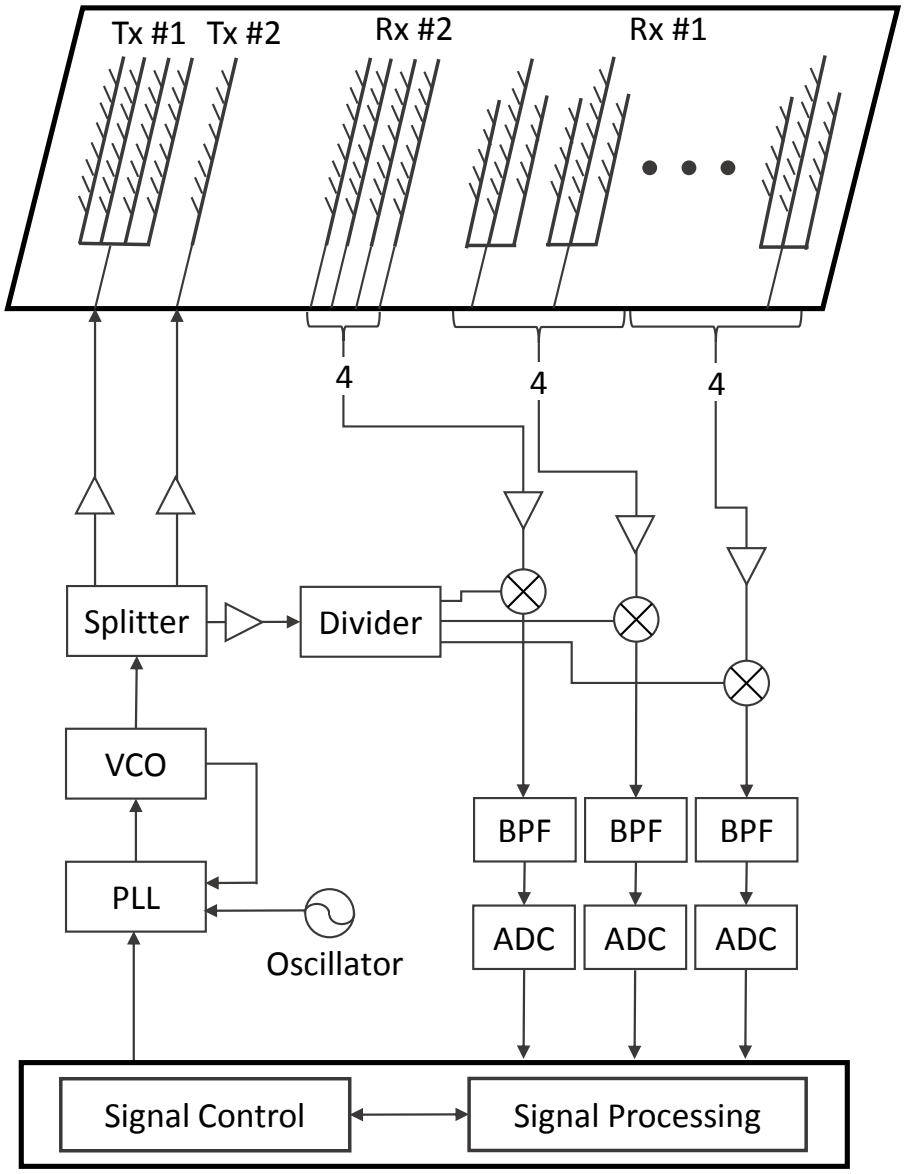

Figure 2.1: Radar system architecture of an MBMR radar.

Table 2.1: System requirements of MBMR radar

Parameter	Value	
	LRR	SRR
Frequency	$76 - 77GHz$	
Average transmit power	$\leq 10mW$	
Cycle time	$\leq 100ms$	
Detection range	$1 - 200m$	$1 - 60m$
Detection velocity	$-360 - +180kph$	
Field of view	$\geq 20°$	$\geq 60°$

Table 2.2: System parameters of MBMR radar

Parameter	Value	
	LR R	SRR
Modulation type	FMCW	
Bandwidth (B)	500 MHz	750 MHz
Chirp duration (T)	5 ms	2.5 ms
Sampling rate (f_s)	400 kHz	
Number of antenna	8	4
Antenna spacing	1.8λ	0.6λ
Antenna HPBW	7.1°	42.3°

Table 2.2 summarizes system parameters of proposed 77 GHz MBMR radar. The modulation type is frequency modulated continuous wave (FMCW) commonly. The bandwidth for LRR and SRR is $500MHz$ and $750MHz$ respectively. The range resolution can be calculated as follows,

$$\Delta R_L = \frac{c}{2B_L} = \frac{3 \times 10^8 m/s}{2 \times 500MHz} = 0.3m, \tag{2.4}$$

$$\Delta R_S = \frac{c}{2B_S} = \frac{3 \times 10^8 m/s}{2 \times 750MHz} = 0.2m, \tag{2.5}$$

where ΔR_L and ΔR_S denote the range resolution for LRR and SRR respectively, and B is the sweep bandwidth of the transmitted signal. The chirp duration is $5ms$ and $2.5ms$ respectively and the velocity resolution can be computed as follow,

$$\Delta V_L = \frac{\lambda}{2T_L} = \frac{0.0039m}{2 \times 5ms} = 1.4kph, \tag{2.6}$$

$$\Delta V_S = \frac{\lambda}{2T_S} = \frac{0.0039m}{2 \times 2.5ms} = 2.8kph, \tag{2.7}$$

where T_L and T_S are chirp duration for LRR and SRR, respectively.

The half power beamwidth (HPBW) can be calculated by [23] as follows,

$$HPBW_L = 2 \times sin^{-1}\left(\frac{\lambda}{2\pi d_L} \cdot \frac{2.782}{M_L}\right) = 3.53(^\circ), \tag{2.8}$$

$$HPBW_S = 2 \times sin^{-1}\left(\frac{\lambda}{2\pi d_S} \cdot \frac{2.782}{M_S}\right) \cdot \frac{180}{\pi} = 21.27(^\circ), \tag{2.9}$$

where M_L is the number of antenna for LRR which is designed as 8 with the antenna spacing (d_L) of 1.8λ, and M_S is the number of antenna for SRR as 4 with 0.6λ spacing (d_S).

2.3 Waveform and Signal Processing Structure Design

A Frequency Modulated Continuous Wave (FMCW) is well-known modulation type for automotive radar. A linear FMCW radar transmits signal whose carrier frequency is linearly changed along the time which is called chirp. The range and velocity information can be obtained from the beat frequency which is the frequency difference between transmitted signal and received signal which is delayed due to the round-trip of the transmitted signal and changed by Doppler effect come from the relative speed. The range and the velocity information of the target is mixed in the beat signal from the single chirp [24]. Typical FMCW waveform for automotive system is composed of two periodic chirps with different slope.

Figure 2.2 shows the proposed FMCW waveform and timing diagram for the operation of RF ICs to cover long range area and short range area, simultaneously. The part of positive slope is called up-chirp and the negative slope part is called down-chirp. The

beat frequency is composed of f_r (which is the difference in the frequencies according to the distance of a target) and f_d (which is due to the relative velocity between the radar and a target) with opposite sign for up-chirp and down-chirp. The beat frequency from the up-chirp (f_{bu}) and down-chirp (f_{bd}) can be expressed as follows,

$$f_{bu} = f_r - f_d \tag{2.10}$$

$$f_{bd} = f_r + f_d. \tag{2.11}$$

f_r and f_d can be calculated using (2.12) and (2.13), respectively, $i.e.$,

$$f_r = \frac{2B}{cT}R \tag{2.12}$$

and

$$f_d = \frac{2f_c}{c}V_r = \frac{2}{\lambda}V_r \tag{2.13}$$

where B is the bandwidth, T is the chirp duration, c is the speed of light, f_c indicates the center frequency, and R and V_r are the distance and relative velocity, respectively. The time, which is called a $scan$ consists of the transmission, reception, and signal processing. A single scan duration is $50ms$ long. Identical signals for LRR and SRR are transmitted at every scan, respectively. The transmitted signals for LRR and SRR are separated in time and the received signals are processed serially within a single scan.

Figure 2.3 illustrates the block diagram of the signal processing. First of all, received signal from the ADC is handled with basic signal processing in time domain such as DC offset suppression due to the direct conversion of the FMCW signal, low-pass filtering to reduce the noise outside the effective frequency band, interference mitigation algorithms to recognize the existence of interference from other radar and

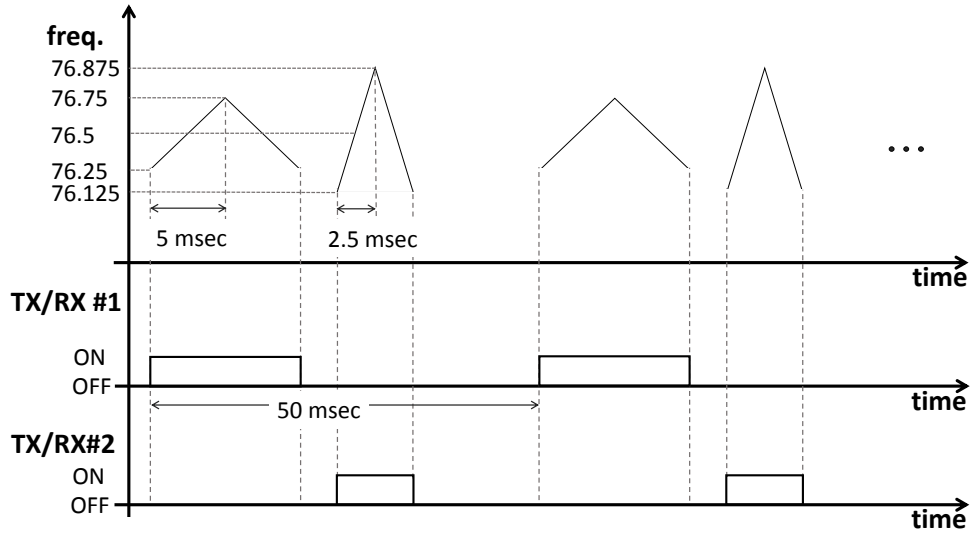

Figure 2.2: Waveform and time diagram of transmitting signal.

enhance the contaminated raw data if the interference exists, and windowing before the Fast Fourier Transform (FFT).

The enhanced time domain signal is converted to the frequency domain signal by FFT, and the rest of the signal processing blocks are dealt with frequency domain signal. The FFT is applied to each receiving channels, respectively, and the digital beamforming is conducted to increase RX antenna gain and widen the coverage in FOV of the TX antenna. We can obtain the spectrum in the frequency domain taking the absolute value of the results of digital beamforming and the frequency peaks in the spectrum can be extracted through peak detection algorithm such as constant false alarm rate (CFAR) algorithm. To obtain more accurate frequency of the frequency peaks, the frequency estimation such as weighted mean, second order polynomial is carried out using frequency indices and magnitude values.

The angle information of each frequency peaks is calculated mostly by conven-

tional beamforming algorithm among various direction of arrival (DOA) estimation algorithms [25]. Frequency peaks having angle information from the up-chirp signal and the down-chirp signal are combined together by comparing the angle, magnitude, and pattern of spectrum. There can exist multiple frequency peaks satisfying various conditions simultaneously which generate ghost targets due to the multiple combination of frequency peaks from the up and down-chirp signal. The pairing is laborious process to prevent ghost targets using various information. Remaining ghost targets are filtered by the tracking algorithm using Kalman filtering.

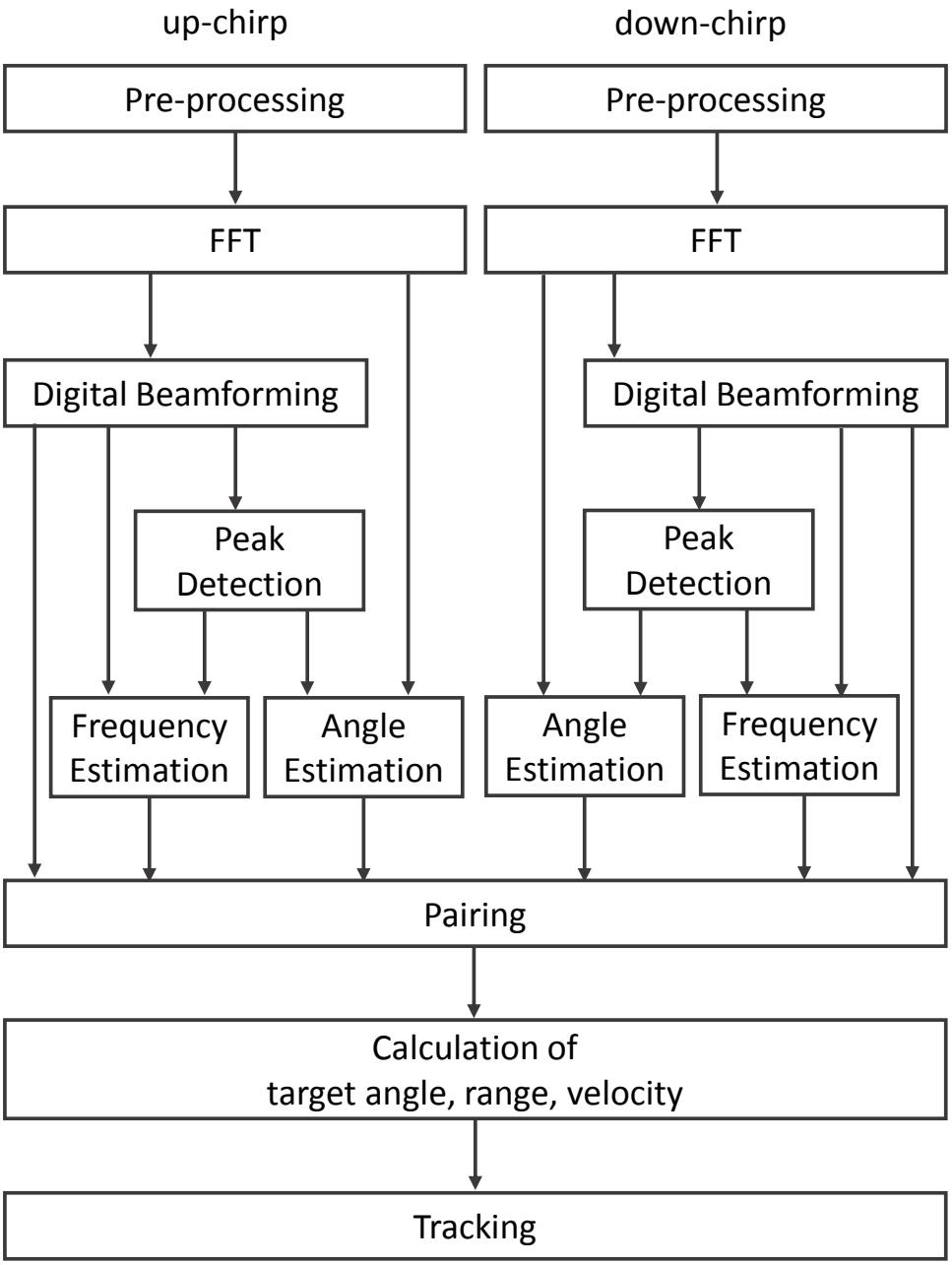

Figure 2.3: Signal processing architecture of an FMCW radar.

2.4 Advanced Singal Processing Technique for AEB

The detection performance of the proposed MBMR radar for ACC is satisfied with the FMCW waveform described in Section 2.3. However, the detection performance in not enough for AEB which need to guarantee the detection ability for stationary targets in close range. The proposed MBMR radar does not have I/Q channels at receiver, thus the direction of detected target is ambiguous. The beat frequency of up-chirp from a target in short range is folded to the positive low frequency region and low frequency region around DC is suppressed to reduce DC and low frequency noise due to the direct conversion of FMCW signal. The extracted beat frequency folded from negative frequency generate objects with different velocity from real targets and the beat frequency not extracted from up-chirp is not paired with beat frequency from down-chirp. False target or missing target in short range can cause dangerous situation under AEB scenario.

To overcome the limitation of the detection capability, we propose an additional down-chirp signal with different slope. Figure 2.4 demonstrates the improved FMCW waveform to fulfill the requirement of the detection performance for AEB. The beat frequency of up-chirp is shifted to low frequency band by the Doppler effect when the relative velocity is negative, thus, we added down-chirp to avoid ambiguities in low frequency band. To differ the slope of the chirp signal, we chose the bandwidth as $750MHz$ which is steeper than existing signal for better frequency extraction avoiding DC region.

We improve the detection performance of the proposed MBMR radar for AEB without change of hardware. This is very important factor for the value added function maintaining production cost. The cycle time including additional modulation and

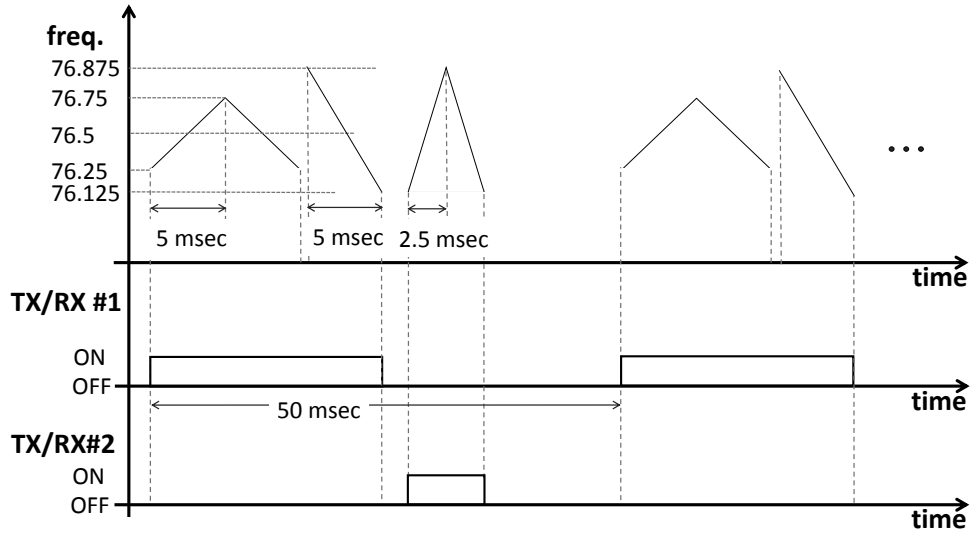

Figure 2.4: Waveform and time diagram of transmitting signal for AEB.

signal processing remains under $50ms$ by the optimization of DSP.

2.5 Design Results

Figure 2.5 shows the photograph of designed RF PCB consists of RF antenna part and RF circuit part. The proposed design concept assembled together to reduce the sensor size and the cost. To prevent the mutual coupling, the cavity which is designed to block RF signals from antennas and RF circuits each other is installed on the RF circuit part.

The antenna of TX#1 is composed of 8 arrays with the power ratio of Dolph-Chebyshev to suppress sidelobes and the power divider is designed to avoid sharp edges to mitigate unexpected losses or reflection at ports. The TX#2 antenna consists of 2 array to cover wide FOV having adequate gain. The antenna spacing of RX# is 1.8λ as mentioned, and each channel has 3 arrays to obtain high antenna gain and sharp beam pattern. An array in the middle of 3 arrays is longer than other arrays to have

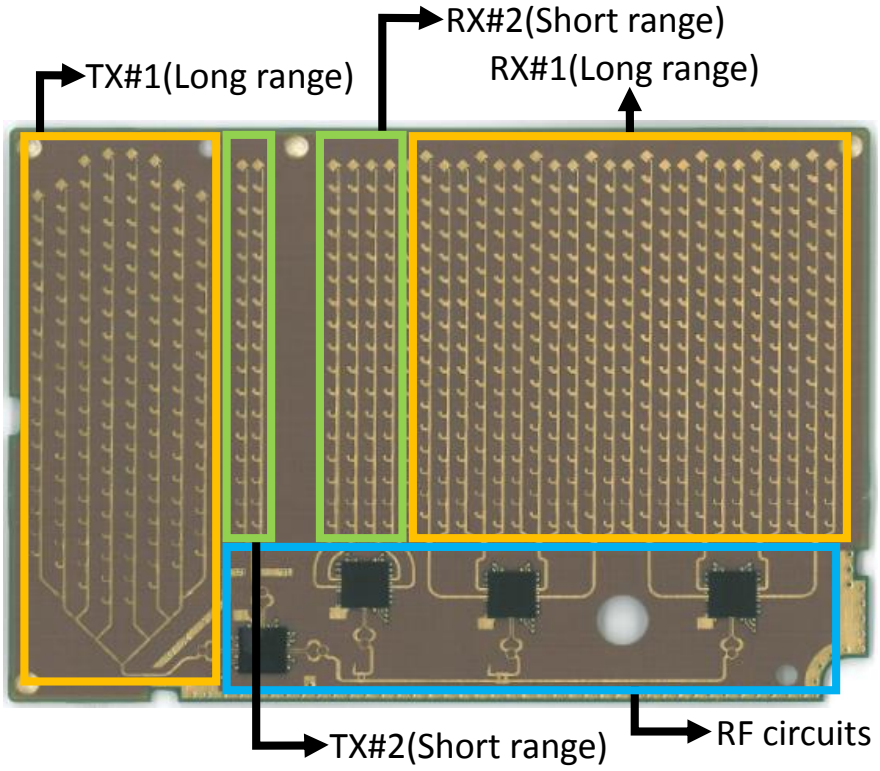

Figure 2.5: Design result of RF PCB board.

stable beam pattern by the spatial windowing effect. The RX#2 antennas are simple single array.

Figure 2.6 demonstrates the radiation pattern of TX#1 antenna. We can confirm that the radiation pattern in the azimuth plane in Figure 2.6a and the elevation plane in Figure 2.6b. The peak gain is 22.23 dBi, the 10 dB beam width in the azimuth is $18.78°$, and the 6 dB beam width in the elevation is $5.27°$. The sidelobe level (SLL) is -25.88 dB and -23.17 dB, respectively. The reason of the specification in the azimuth plane at 10 dB beam width is to suppress grating lobe due to the antenna spacing. The radiation patterns are stable to the frequency band. Similarly, the radiation pattern of

the TX#2 antenna is shown in Figure 2.7, and the azimuth and elevation pattern are also illustrated in Figure 2.7a and Figure 2.7b. The peak gain of the TX#2 antenna is 16.72 dBi, the 10 dB beam width in the azimuth is $86.15°$, and the 6 dB beam width in the elevation is $5.92°$. The SLL is -19.42 dB in the elevation plane. The elevation beamwidth of TX#2 is wider than TX#1 due to the shorter array elements by the integration of RF circuits. This factor is not a problem because of the detection range of SRR is much shorter than that of LRR but an advantage in terms of AEB detecting close pedestrians which are oblong shape.

2.6 Experimental Results

2.6.1 Anechoic Chamber

Experiments to confirm the basic detection performance of the proposed MRMR radar were carried out in an RF anechoic chamber with Radar Target Simulator (RTS) which can generate reflected signal of a target as depicted in Figure 2.8. The MBMR radar is installed on a turn table which can rotate the radar to azimuth and vertical direction. We can obtain beam pattern of receiving channels and verify the signal processing for detection with the RTS and the turn table. Figure 2.9 shows measurement results of angular power spectrum in the chamber. The obtained beamwidth from Figure 2.9a to Figure 2.9c is very narrow in LRR region. There exist grating lobes in LRR angular power spectrum, however, grating lobes are suppressed by TX radiation pattern in Figure 2.6a outside the FOV of LRR region. The beamwidth of Figure 2.9d and Figure 2.9e is wide in SRR region. The angular accuracy is under $0.5°$ in the entire FOV.

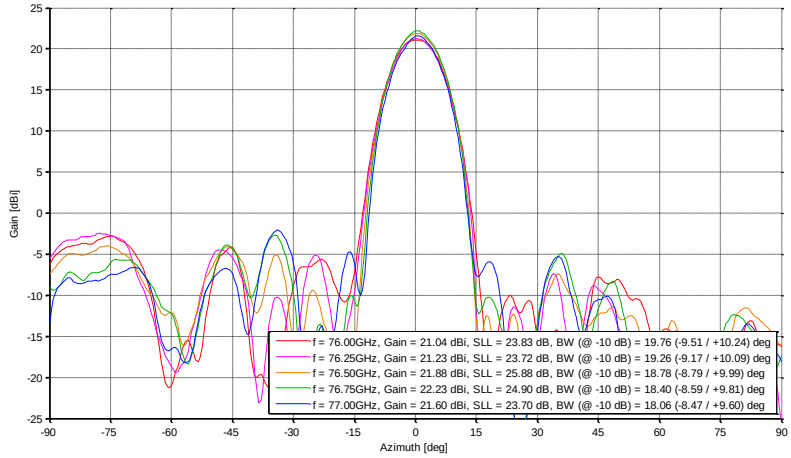

(a) Measured radiation pattern in azimuth the plane

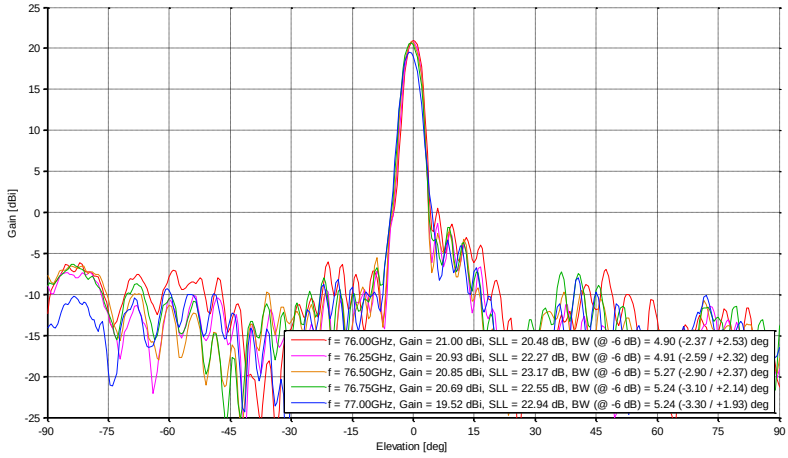

(b) Measured radiation pattern in elevation the plane

Figure 2.6: Measurement of radiation pattern of TX#1 antenna.

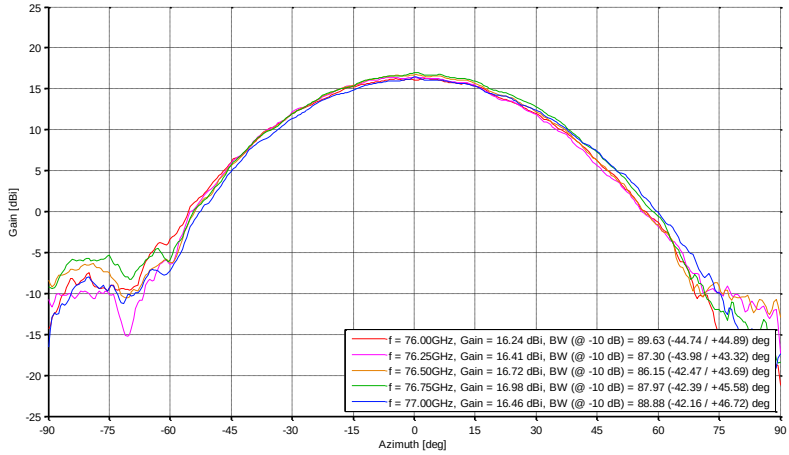

(a) Measured radiation pattern in azimuth the plane

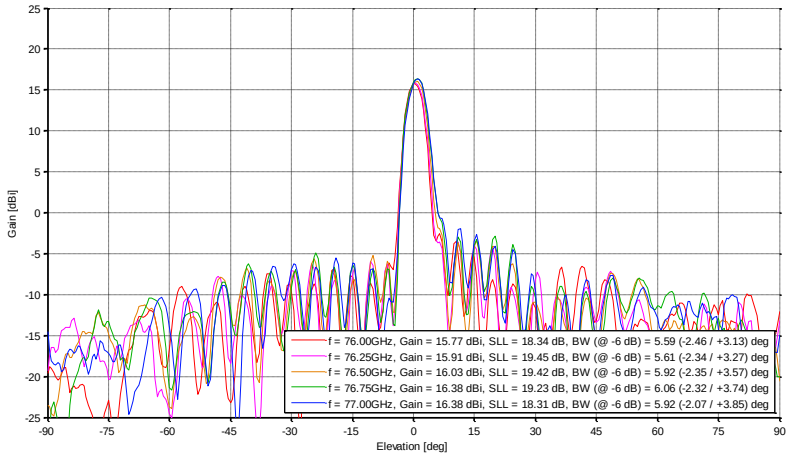

(b) Measured radiation pattern in elevation the plane

Figure 2.7: Measurement of radiation pattern of TX#2 antenna.

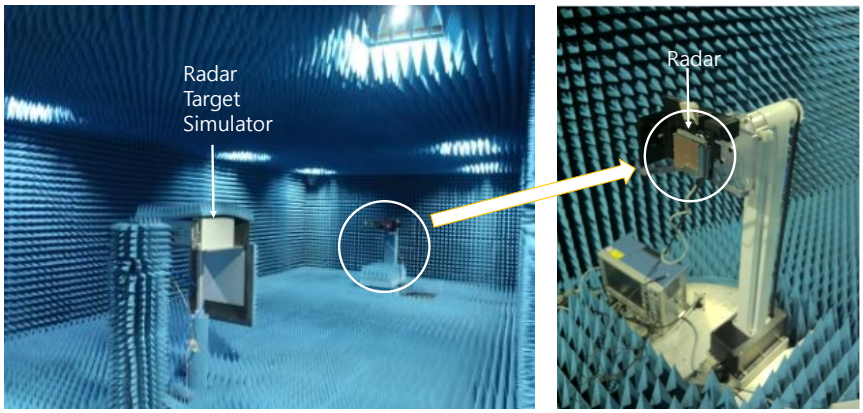

Figure 2.8: RF anechoic chamber with target simulator.

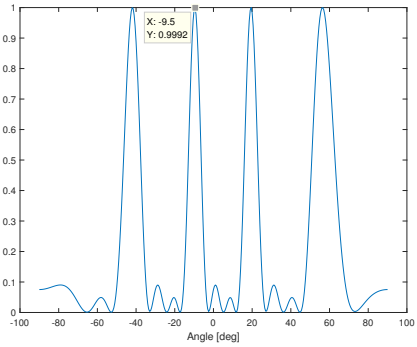

(a) Target angle : -10°

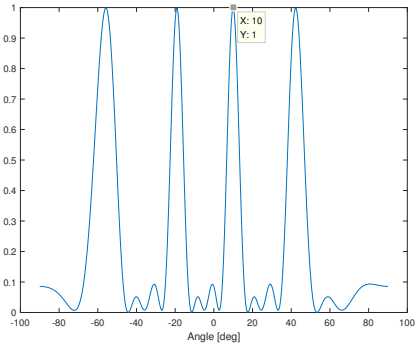

(b) Target angle : 10°

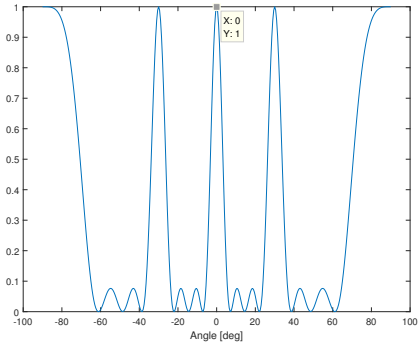

(c) Target angle : 0°

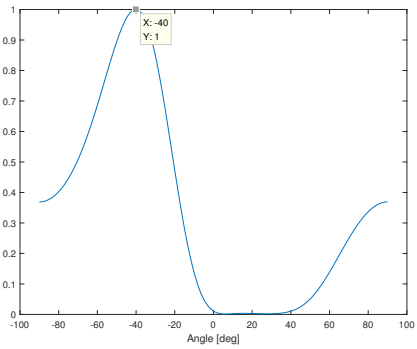

(d) Target angle : -40°

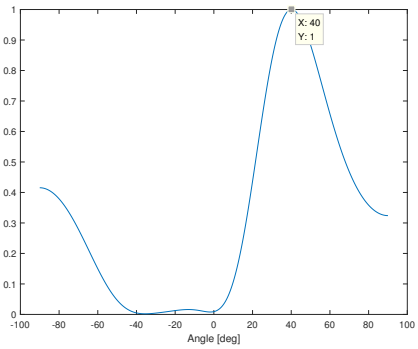

(e) Target angle : 40°

Figure 2.9: Measurement result of angular power spectrum.

Figure 2.10: Test vehicle installed MBMR radar.

2.6.2 Field Test

The proposed 77 GHz MBMR radar was installed in front of the test vehicle which is Grandeur HG from Hyundai Motors Company as in Figure 2.10 to perform experiments on roads. The detection coverage test was conducted at open space and the test scenario is illustrated as left figure in Figure 2.11. The test vehicle installed radar is stopped at the center lane and the target vehicle was slowly driven forward in front of the test vehicle until the range of $200m$ and repeated experiments at left and right side lanes. The experimental results in right-side of Figure 2.11 satisfy the detection specification in LRR and SRR area. We can confirm that the detection range reach to $200m$ in LRR area and to $\pm 40^{\circ}$ in SRR area.

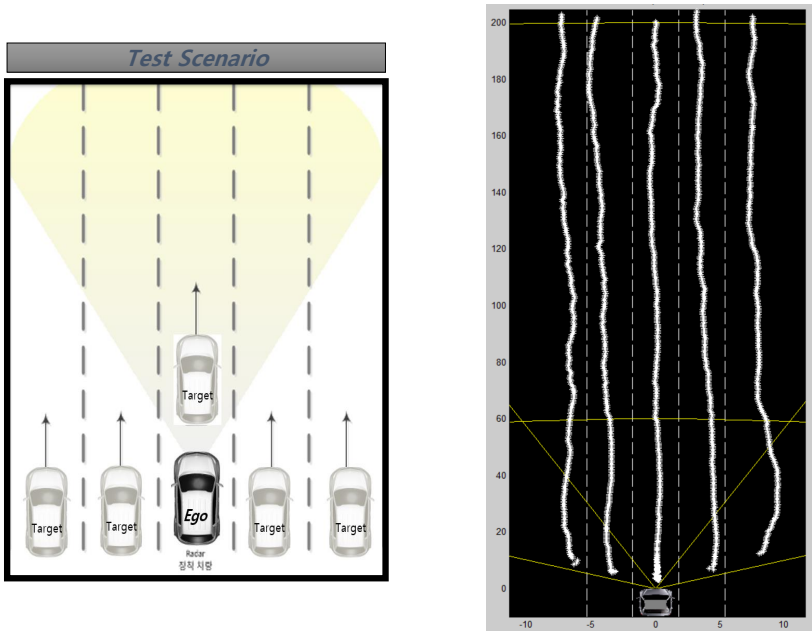

Figure 2.11: Test scenario and result of the detection coverage performance.

2.7 Summary

In this chapter, we have proposed an advanced multi-beam and multi-range automotive radar for ACC and AEB. Based on the theoretical background, system parameters were designed to fulfill the system requirement, and an efficient hardware structure was proposed for the actual implementation. The signal processing structures optimized for the proposed hardware were designed and implemented as an embedded software. In order to verify the detection performance of the radar, basic tests are performed in RF anechoic chamber using RTS. The detection results of range, velocity, and angle information were properly extracted from the radar. To confirm the detection coverage performance, we performed field test in the open space using test vehicle. The detection result have satisfied with the system requirement.

Chapter 3

Iron-tunnel Recognition

3.1 Introduction

As concern for safety and driver assistance increases, various safety sensors are being introduced for automobiles. Because radar, among many sensors shows robust performance under bad weather conditions or poor road environments, the installation rate of automotive radar all over the world is rapidly increasing. As issues for autonomous emergency braking or autonomous driving for safety become crucial in the near future, the needs for autonomous radar sensors will explosively grow [4]–[2]. As the automotive radar becomes popular, adaptive cruise control (ACC) [6] with radar becomes one of the functions with the highest utility for convenience of driver. Using the ACC function, drivers can reduce fatigue during driving as well as be assured of safety even though the visibility is poor because of bad weather condition. However, if structures such as an iron tunnel or a soundproof wall reflect considerable electromagnetic waves, undesired clutter signal may appear to be larger than signal reflected from the target, resulting in the deterioration of the radar detection performance. In this case, sensing robustness, which is the advantage of automotive radar, may not be guar-

anteed. Because hardware resources for enhancement of radar detection performance are limited, implementation of a signal processing technique is necessary to overcome performance deterioration due to the road environment.

A few studies on the reflection and diffraction on road surfaces have been conducted for automotive radar sensors [8]–[10]. These studies have found that the radar detection performance is dependent on surface condition and slope of roads. Meanwhile, few research works on the clutter structure on roads have been reported [11], [12]. These studies are based on ultra wideband pulse radars, so that applying them to other modulation such as frequency-modulated continuous wave (FMCW) radar [13]–[15] is inadequate. In addition, some approaches to differentiate structures such as a bridge or a guardrail from stationary objects on the road have been studied [16]–[18]. However, most studies did not consider the situation in which structures, such as iron tunnels, with large reflection are densely distributed.

In this chapter, we propose a novel iron-tunnel recognition method to overcome the deterioration in the target or vehicle detection performance due to iron tunnel clutters. The proposed method recognizes an iron tunnel by analyzing the spectrum characteristics of the received radar signal under different road conditions. We observed that an iron tunnel causes a high intensity scattering over a wide frequency band. Thus, the proposed method measures the degree of spectral spreading by incorporating the entropy concept. The experimental data used in this paper are obtained from a 77-GHz forward-looking FMCW radar for ACC. We demonstrate that the proposed method can successfully detect iron tunnel. In addition, the results show that the missing problem of a target vehicle in an iron tunnel under ACC using radar is improved by overcoming the deterioration in the detection performance around or inside iron tunnels.

This chapter is organized as follows: In Section 3.2, the description of the radar

model used in the research and the analysis of the spectral characteristics of the received signal in accordance with various road environments are explained. Then, the proposed method is presented in detail. In Section 3.3, the experimental results of recognizing an iron tunnel as well as the results that show the improvement in the ACC performance are provided. Finally, we summarize and conclude our works in Section 3.4.

3.2 Iron-Tunnel Recognition

In this section, we briefly explain and mathematically describe the radar model. Then, the spectral characteristics of the radar signal under various road conditions are presented. A novel method to recognize an iron tunnel based on the spectrum spreading characteristics is proposed.

3.2.1 Radar Model

We have exploited a 77-GHz forward looking FMCW long-range radar. Fig. 3.1 shows the structure of the FMCW radar. It consists of the antenna module where an electrical radio frequency (RF) signal is converted to an electromagnetic wave, the transceiver unit that generates the RF signal and processes the received RF signal, and the signal control and processing unit that controls the RF signal and processes the received signal. The antenna module contains the linear patch array antenna which implemented on the printed circuit board. The signal control and processing unit handles schedule of FMCW modulation and radar scanning. The transmission channel is a single channel, and the receiving channel consists of K uniform linear arrays. The time, which is called a $scan$ consists of the transmission, reception, and signal processing. A single

$scan$ duration is 50 ms long. Identical signals are transmitted at every $scan$. If the signal transmitted from the FMCW radar is reflected by L targets, the received signal in the kth array is defined as

$$s_k(t) = \sum_{i=0}^{L-1} A_k(i) cos\big(2\pi f(i)t + \phi_k(i)\big). \tag{3.1}$$

$A_k(i)$ is the amplitude of the signal reflected from each target at the kth antenna. $\phi_k(i)$ is the phase component of the each received signal. $f(i)$ is composed of $f_r(i)$ (which is the difference in the frequencies according to the distance of a target) and $f_d(i)$, (which is due to the relative velocity between the radar and each target). $f_r(i)$ and $f_d(i)$ can be calculated using (4.2) and (4.3), respectively, $i.e.$,

$$f_r(i) = \frac{2B}{cT} R(i) \tag{3.2}$$

and

$$f_d(i) = \frac{2f_c}{c} V_r(i) = \frac{2}{\lambda} V_r(i) \tag{3.3}$$

where B is the bandwidth, T is the chirp duration, c is the speed of light, f_c indicates the center frequency, and $R(i)$ and $V_r(i)$ are the distance and relative velocity, respectively. $s_k(n)$ is the discrete-time signal of $s_k(t)$ and can be expressed as

$$s_k(n) = \sum_{i=0}^{L-1} A_k(i) cos\big(2\pi f(i)n + \phi_k(i)\big) \tag{3.4}$$

where $n(0 \leq n < N)$ is the discrete-time index of the received signal during a single $scan$ and N is the total number of samples in a single $scan$.

If these received signals are transformed using the short-time Fourier transform (STFT), they can be expressed as

$$S_k(f, m) = \sum_{n=0}^{N-1} s_k\big(n + (m-1) \cdot N\big) e^{-j\frac{2\pi f}{N} \cdot n} \tag{3.5}$$

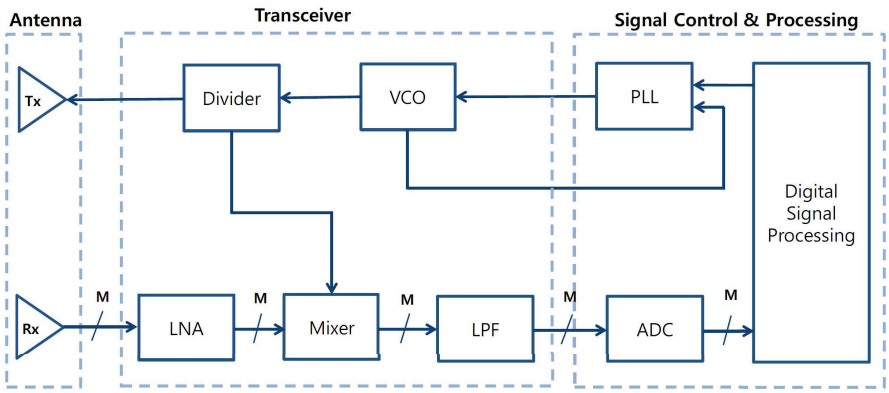

Figure 3.1: Radar system architecture.

where f is the frequency index and m is the $scan$ index. The magnitude response in the frequency-domain can be obtained as

$$P(f,m) = \left| \sum_{k=0}^{K-1} S_k(f,m) \right|. \tag{3.6}$$

3.2.2 Spectral Characteristics of an Iron-Tunnel

To understand the characteristics of the radar signal affected by an iron tunnel, we analyzed its spectral characteristics. To extract only the frequency characteristics of an iron tunnel, we investigated the frequency characteristics using the signal acquired at a normal road, an expressway, and the entry of and inside an iron-tunnel. Fig. 3.2 shows the magnitude response using the STFT of the received signal under various road conditions. Fig. 3.2a shows high intensity (red color) in the 20-30-kHz frequency band under normal road condition, which means that a single target with almost the same velocity as the ego-vehicle exists at the front. The light green or yellow diagonal lines correspond to vehicles with different velocities from the ego-vehicle or stationary objects such as road sign. Fig. 3.2b shows an expressway condition, and similar to Fig. 3.2a, the target vehicle has a high intensity over the entire spectrum. The phe-

nomenon that has a high intensity at a constant frequency band means the relative velocity of the ego-vehicle and the target remains constant. Fig. 3.2c shows the entry point of an iron tunnel, and initially ($t < t_0$), a high intensity appears at the narrow frequency bands. The high-intensity is observed over a wide frequency bands as the vehicle approaches the tunnel. Fig. 3.2d shows the condition inside the iron tunnel, and the high intensity response is observed over the entire band due to the iron structure inside the tunnel. The iron tunnel causes the spectral response in the wider frequency bands. Thus, if the spectrum spreading of the received signals can be quantitatively measured, an iron tunnel can be recognized.

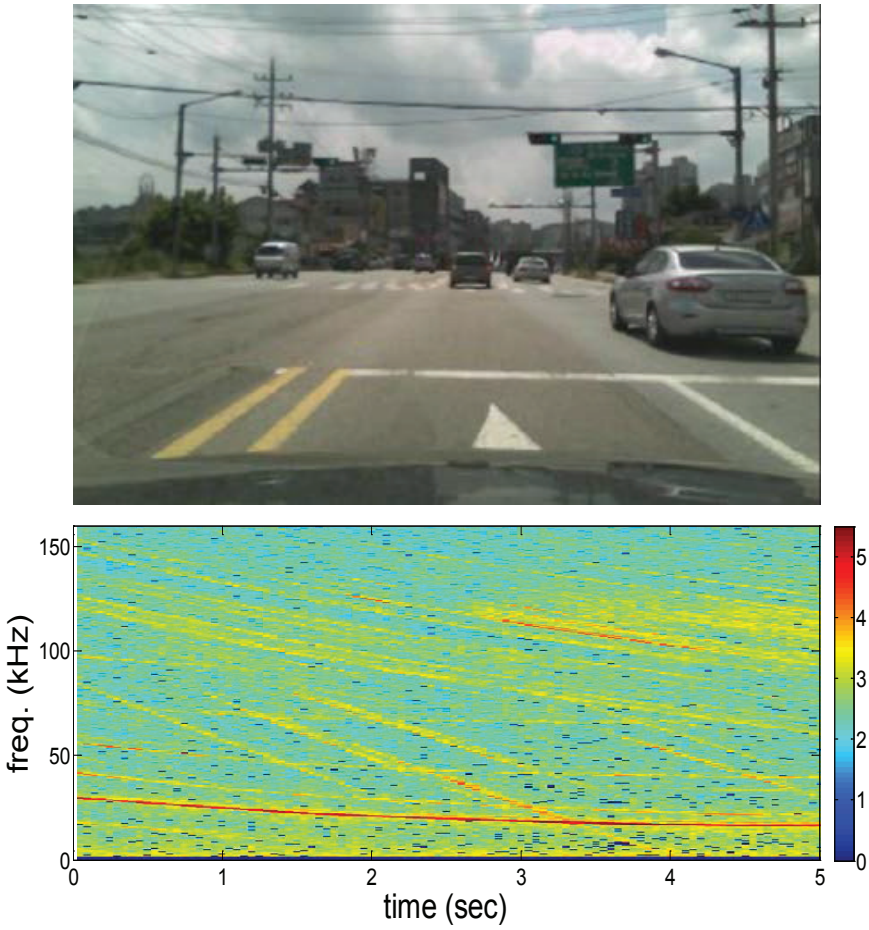

(a) Normal road

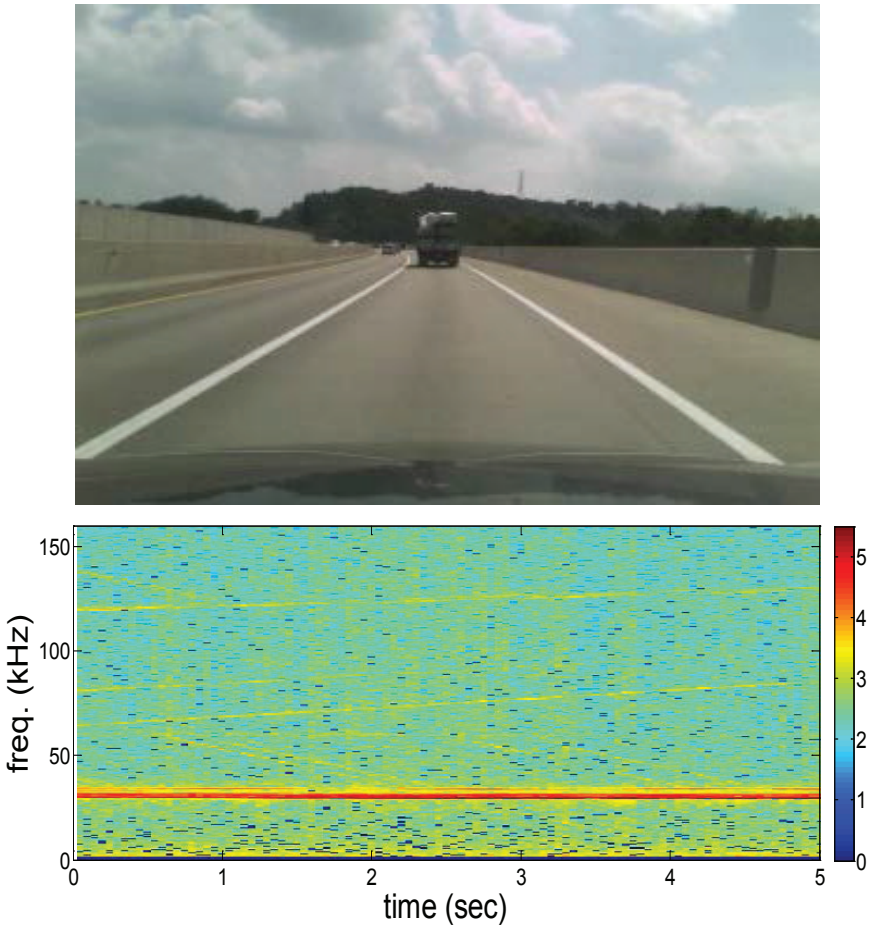

(b) Expressway

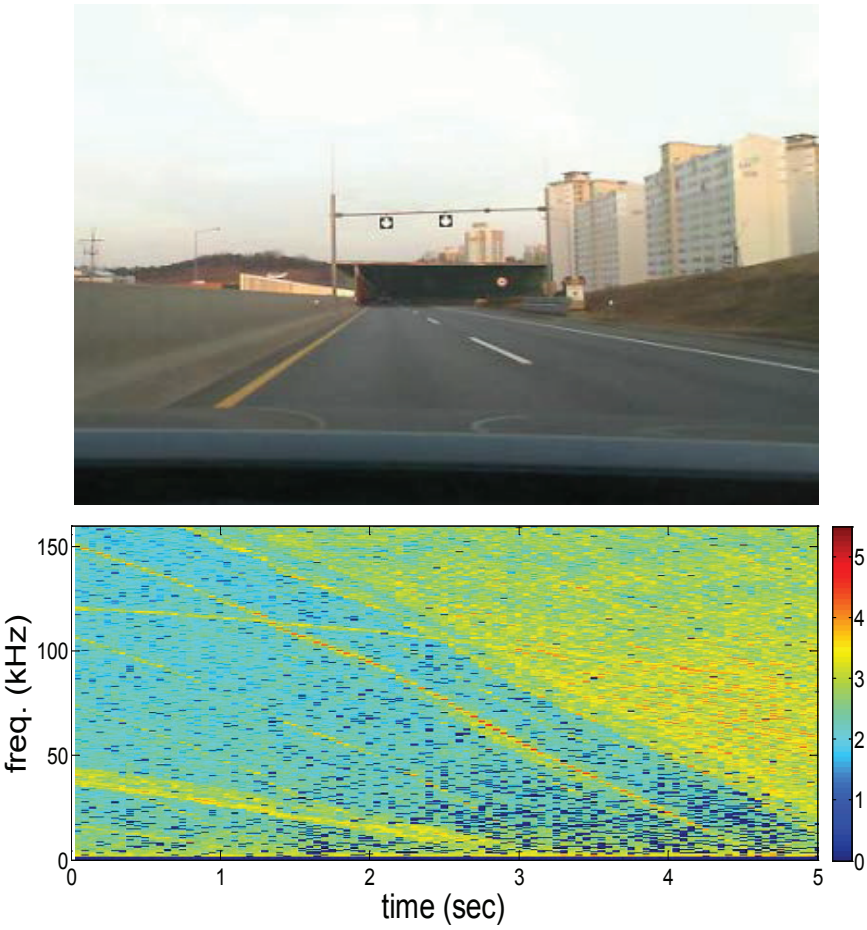

(c) Entry of iron-tunnel

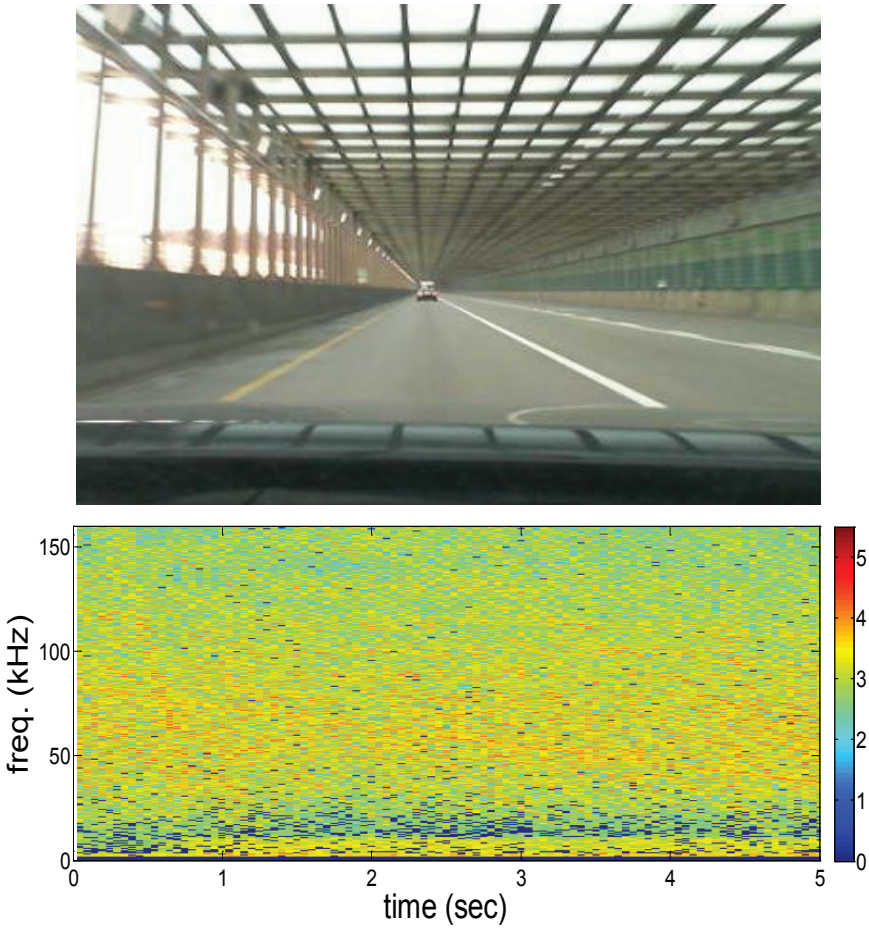

(d) Inside iron-tunnel

Figure 3.2: Spectrogram of the received radar signal under various road conditions.

3.2.3 Measuring Spectrum Spreading

To recognize an iron tunnel as mentioned above, a quantitative measurement of the degree of spectrum spreading is necessary. To achieve this objective, the standard deviation of the spectrum spreading can be preferentially considered. The standard deviation can be used as a measure of the spectrum spreading by calculating the frequency magnitude response as

$$\sigma(m) = \sqrt{\frac{1}{N}\sum_{f=0}^{N-1}\left(P(f,m) - \overline{P(f,m)}\right)^2} \tag{3.7}$$

where $\overline{P(f,m)}$ is the average value of the magnitude response with respect to frequency. In general, the more the data are not evenly distributed i.e. the larger the value of the difference from the average value, the larger is the standard deviation. However, the standard deviation is very sensitive to impulsive components and violent fluctuation in the data.

In this paper, we propose a new method that can measure spectrum spreading using the concept of entropy. Shannon entropy(SE) is generally used to measure the uncertainty of information, and it can be represented as follows

$$SE = -\sum_{i=0}^{N-1} p(i)\log_2 p(i). \tag{3.8}$$

Here, $p(i)$ is the probability density function. If the frequency magnitude response is diffused across a wide band, $p(i)$ is uniformly distributed, and in this case, SE is expected to have a large value. In contrast, when $p(i)$ is concentrated in a narrow frequency bands, the probability distribution of the magnitude is narrow, and SE has a small value. The proposed method measures the degree of spectrum spreading by calculating SE using the probability distribution of the frequency magnitude. To obtain the probability distribution of the magnitude of the frequency response of the received

signal, we define $p_m(i)$ as

$$p_m(i) = \frac{(number\ of\ samples\ per\ scan \in B_i)}{N},\ (0 \leq i < I) \tag{3.9}$$

where $B_i = \{P(f,m)|P_{max} \cdot \frac{i}{I} \leq P(f,m) < P_{max} \cdot \frac{(i+1)}{I}\}$ and P_{max} is the largest value of $P(f,m)$. Thus $p_m(i)$ is the ratio between the number of samples found within interval B_i and the total number of samples N in the mth $scan$. The proposed spectrum spreading measure can be expressed as

$$S(m) = -\sum_{i=0}^{I-1} p_m(i) \log p_m(i). \tag{3.10}$$

The frequency response of the radar signal in a normal road situation may have a number of frequency peaks due to the signal reflected from various targets. When many vehicles or static objects are present on the road, the frequency components due to the target are distinct, and the frequency peak numbers are proportional to the number of targets. Therefore, the time-frequency spectrum may show concentrated peaks in several particular bands, and the spectrum spreading measure SE becomes small. On the other hand, because the iron structures are densely distributed in an iron tunnel, time-frequency spectrum is widely distributed. Also the intensity of the reflected signal varies depending on the distance even if the structures are made of the same material due to the attenuation difference of the reflected signal. In addition, because the iron structures do not exist on the same azimuth plane as the ego-vehicle and they are distributed in different angles in the elevation direction of the iron structure, a discrepancy in the intensity of the reflected signal exists. Therefore, intensity distribution of the time-frequency spectrum of the reflected radar signal exists in wider frequency bands and the spectrum spreading becomes larger. The origin of the spectral spreading is not UWB nature but the dense multipath scenario in iron-tunnels since we have performed experiments using 77-GHz FMCW radar.

To provide a better insight of the spectrum spreading in an iron tunnel, we provide two examples. Table 3.1 lists the latitude and longitude coordinates, the timing of the entrances, and the length of two iron tunnels. The standard deviation in (3.7) and the spectrum spreading measure in (3.10) under the road conditions listed in Table 3.1 are calculated, as shown in Fig. 3.3. Fig. 3.3a shows that both standard deviation and spectrum spreading values in the entry point at approximately 13 s gradually increase. However, the standard deviation in the time point $5s$ before entering the iron tunnel shows a significantly high value, whereas the spectrum spreading measure maintains a relatively steady value. The high fluctuation in the standard deviation may deteriorate the recognition of the iron tunnel. Fig. 3.3b, shows a similar tendency with Fig. 3.3a. However, inside the tunnel, the standard deviation decreases again and fluctuates, and this result may make the recognition of the iron tunnel difficult. On the other hand, the spectrum spreading value is maintained at its high level until leaving out of the tunnel.

Table 3.1: Iron-tunnel profile

Case	Tunnel Entry		Tunnel Length (km)	Experiment Date
	Geographic coordinate (latitude, longitude)	Time (s)		
A	(37.27, 127.08)	15.25	1.0	Jan.27.2014
B	(37.17, 127.03)	4.25	0.7	Feb.05.2014

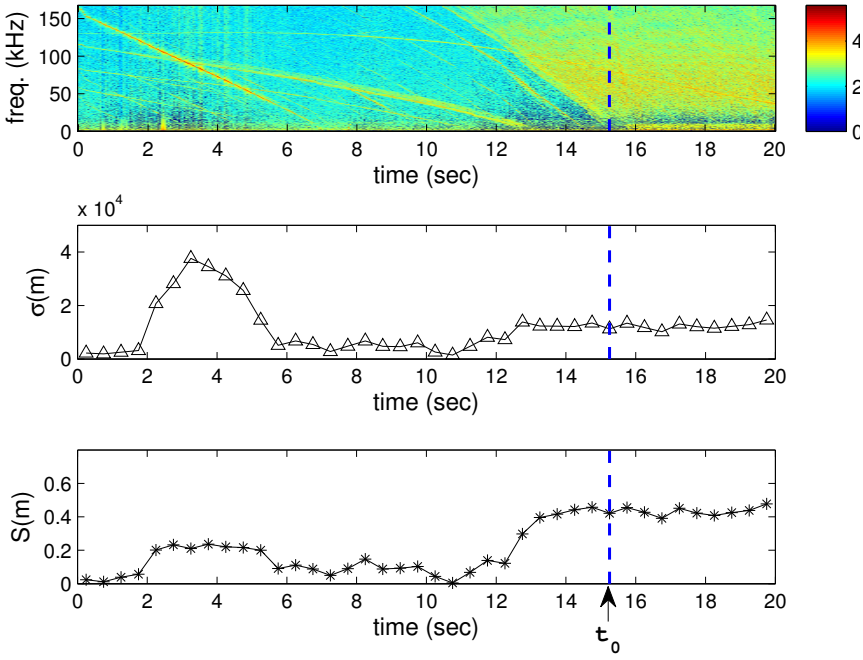

(a) Case A ($t_0 = 15.25$ s)

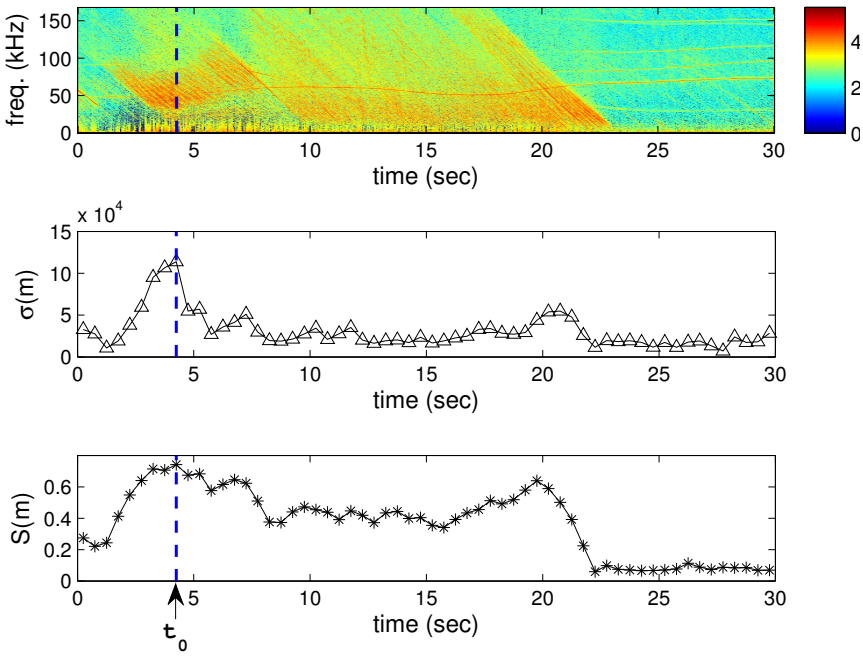

(b) Case B ($t_0 = 4.25$ s)

Figure 3.3: Spectrogram and spectral spreading.

3.3 Experimental Result

In this section, we present the experimental results using measured data in real environment having various iron tunnels to verify that the iron-tunnel recognition method proposed in Sec. 3.2 is feasible. In addition, improvement in the ACC performance in various iron tunnels is presented.

3.3.1 Iron-Tunnel Recognition

To verify that the iron tunnel can be recognized by the proposed spectrum spreading, we tested the proposed method using measured data at various iron-tunnels. The iron-tunnel recognition threshold of the spectrum spreading measure was set to 0.35; if the threshold is exceeded, we considered it as a tunnel. The actual tunnel entry time is indicated by the dotted line, and the tunnel recognition time is indicated by the solid line. Fig. 3.4a shows that the spectrum spreading measure of the normal tunnel is lower than the threshold, namely, 0.35 and thus, it is not recognized as an iron tunnel. Fig. 3.4b–3.4d shows the results obtained by changing the vehicle, radar sample, and experimental date in the two iron tunnels listed in Table 3.1. Fig. 3.4 shows that if the tunnels come within the field-of-view of the radar, they are always recognized as iron tunnel before entering because the signal is received in advance.

Table 3.2 summarizes the latitude and longitude coordinates of the tunnel entrance, tunnel entry time, iron-tunnel recognition time, length of the tunnels, and average value of the spectrum spreading at $2s$ before and after recognition. We can confirm that a significant difference exists between the average values of the spectrum spreading measure before and after the tunnel recognition.

Table 3.2: Spectrum speading and profile of various tunnels

Case	Type	Tunnel Entry		Recognition Time, t_r (s)	Tunnel Length (km)	Spectrum Spreading		Experiment Date
		Geographic coordinate (latitude, longitude)	Time, t_0 (s)			before recognition	after recognition	
A	normal	(37.25, 127.09)	4.00	-	0.3	0.14	-	Oct.08.2013
B	iron	(32.27, 127.08)	15.50	14.00	1	0.23	0.41	Jan.06.2014
C	iron	(32.27, 127.08)	12.25	9.50	1	0.21	0.58	Feb.05.2014
D	iron	(32.17, 127.03)	7.50	3.50	0.7	0.17	0.46	Jan.14.2014

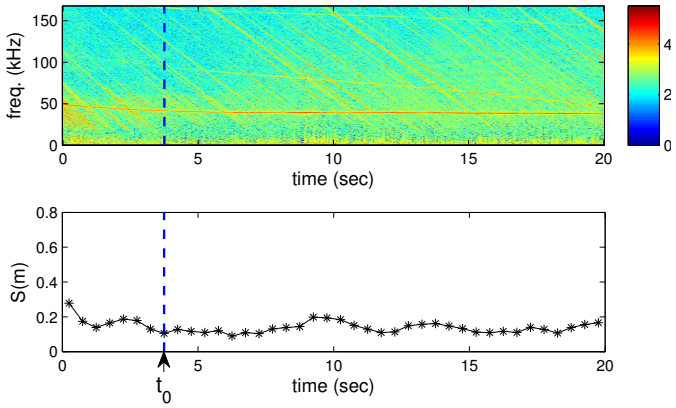

(a) Case A ($t_0 = 4.00s$)

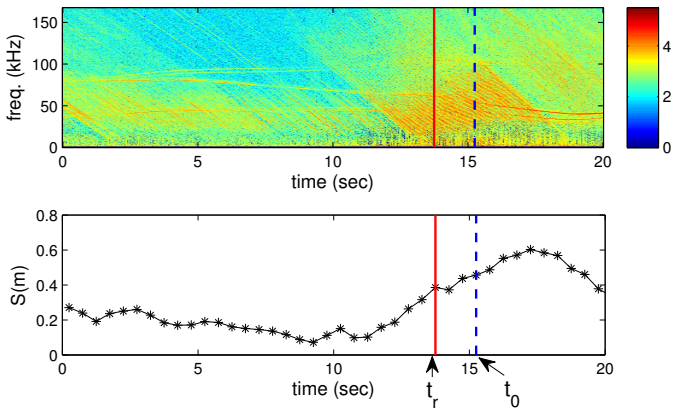

(b) Case B ($t_0 = 15.50s$, $t_r = 14.00s$)

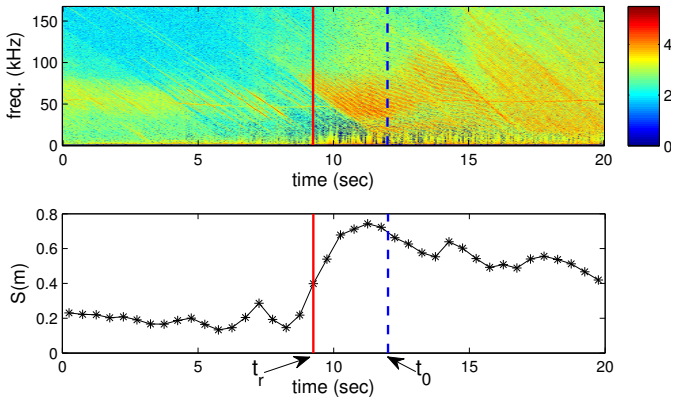

(c) Case C ($t_0 = 12.25s$, $t_r = 9.50s$)

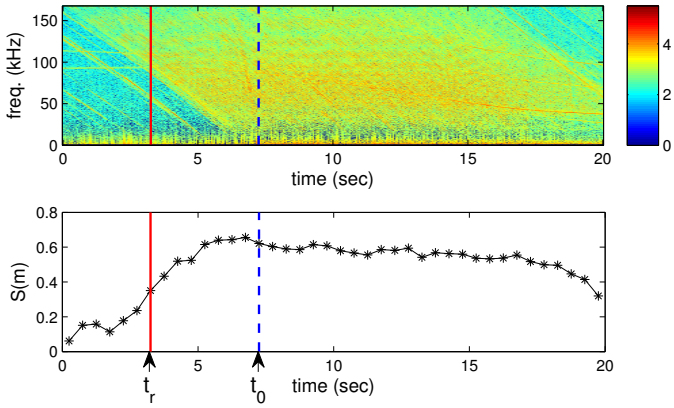

(d) Case D ($t_0 = 7.50s$, $t_r = 3.50s$)

Figure 3.4: Iron-tunnel recognition using the proposed spectral spreading measure (t_0:tunnel entry time, t_r:tunnel recognition time).

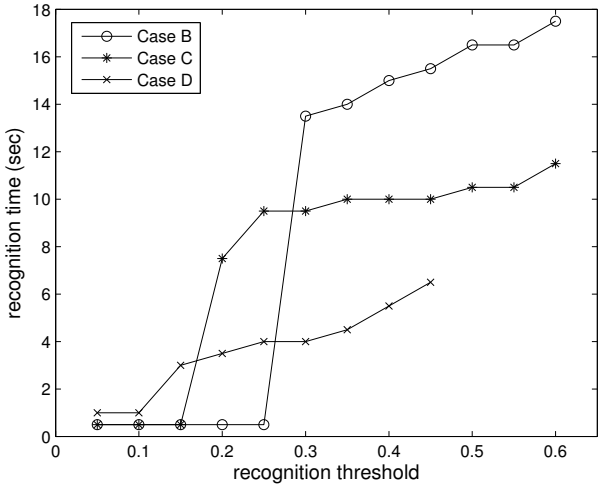

Figure 3.5: Iron-tunnel recognition time according to the recognition threshold

To ensure that the threshold for the iron-tunnel recognition is reasonable, we examined the recognition time of the iron tunnel in terms of the threshold. Fig. 3.5 shows the plot of the iron-tunnel recognition time by changing the detection threshold from 0.05 to 0.7 in increments of 0.05. In Fig. 3.5, we can observe that the detection time increases as the threshold increases. However, for the threshold from 0.3 to 0.5 the detection time is somewhat steady. For case B, C, and D, similar trends are observed, and we consider that the reasonable threshold setting is between 0.3 and 0.45. However, to increase the robustness of the threshold, statistical analysis may be required using more extensive experimental data.

3.3.2 Early Target Detection and Prevention of Target Drop

To examine the usefulness of the proposed iron-tunnel recognition method for ACC, experiments were carried out to determine how quickly targets or vehicles are detected in the lane of the ego-vehicle near an iron tunnel. Fig. 3.6 shows the detection results

with and without applying the iron-tunnel recognition method during the detection of the forward target vehicles after entering the iron tunnel. Fig. 3.6a shows the spectrum spreading for the tunnel recognition, and the tunnel was recognized at $14.25s$. Fig. 3.6b shows the average value of the target detection threshold in frequency domain. The dotted line represents the average value of the threshold calculated by the ordered statistic constant false alarm rate (OS-CFAR) algorithm [26] and the solid line shows the average value of the threshold for target detection adjusted by the proposed iron tunnel detection. As shown in Fig. 6b, the threshold level by OS-CFAR becomes very high due to many clutters in an iron tunnel. This high threshold may lead to miss target vehicles inside an iron tunnel. On the other hand, using the solid line threshold lowered by recognizing an iron tunnel, the risk of target missing can be reduced. Fig. 3.6c shows the detection trajectory of the target vehicle along the distance of motion. We can confirm that when the target detection threshold is adjusted by the iron-tunnel recognition, the target vehicle can be detected at an earlier time. The initial target detection time is a very important factor in the ACC performance. If the target vehicle is detected very late, the accelerating ego-vehicle performs sudden deceleration. Thus, riding condition becomes uncomfortable and the risk of collision may increase if the ego-vehicle speed is high. In addition, sudden deceleration may cause rear collision if the distance between the ego-vehicle and the following vehicle is close. Fig. 3.6d shows the frequency response of the received radar signal at the time ($17.15s$) when a target is first detected after the tunnel recognition, and we can observe that the clutter level is significantly high in the 40-100 kHz range. Because the clutter level near or inside the iron tunnel is higher than the peak of a target vehicle, the target vehicle cannot be detected. Thus, we need to control the target detection threshold by iron-tunnel detection.

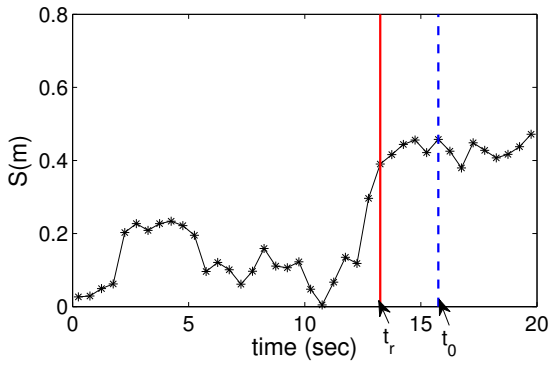

(a) Spectrum spreading

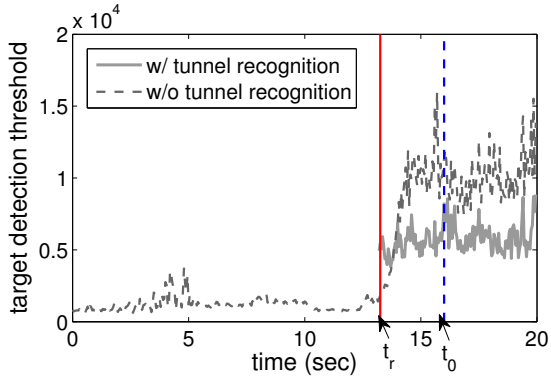

(b) Mean threshold for target detection

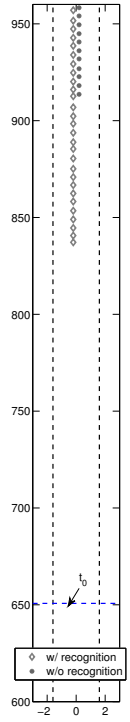

(c) Trajectory comparison of detection result

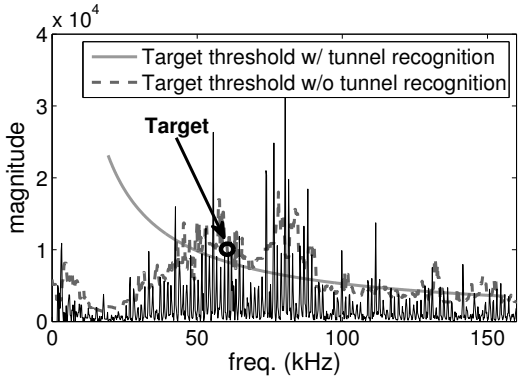

(d) Frequency response at $t = 17.15$ s

Figure 3.6: Comparison of detection result (Early detection) (tunnel entry time, $t_0 = 15.75s$, tunnel recognition time, $t_r = 13.25s$)

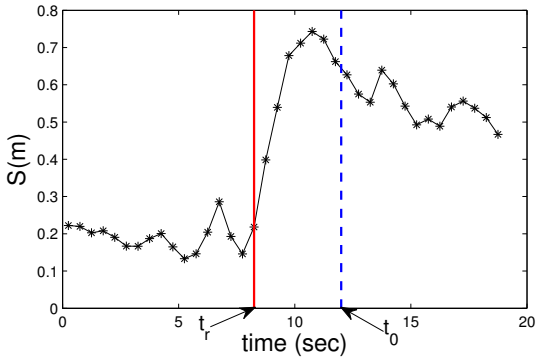

(a) Spectrum spreading

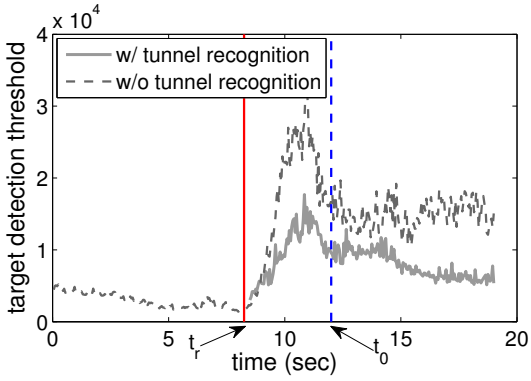

(b) Mean threshold for target detection

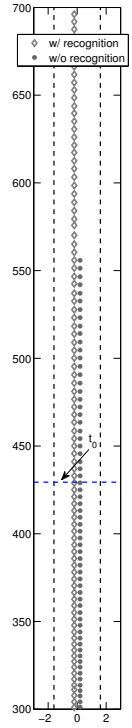

(c) Trajectory comparison of detection result

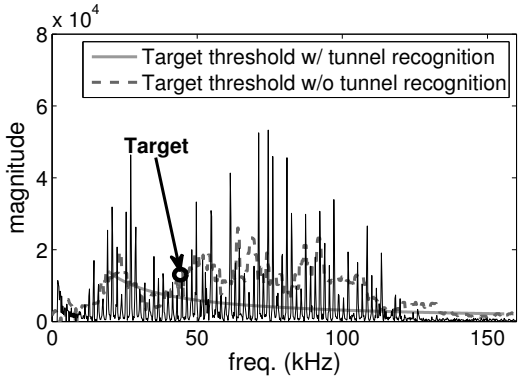

(d) Frequency response of at $t = 13.15s$

Figure 3.7: Comparison of detection result (Early detection) (tunnel entry time, $t_0 = 12.00s$, tunnel recognition time, $t_r = 8.25s$)

To provide another example of the usefulness of the proposed iron-tunnel detection method for ACC, experiments were carried out to determine how reliable the detection by the structure of the iron tunnel is. Fig. 3.7a shows the spectrum spreading measure for the tunnel recognition, and the tunnel was recognized at 8.75 s. Fig. 3.7b shows the average value of the target detection threshold in the frequency domain and the threshold is adjusted similar to that shown in Fig. 3.6. Fig. 3.7c shows the detection trajectory of the target vehicle along the distance without missing targets inside an iron tunnel. We can confirm that the target was not missed in the middle of the trajectory when iron-tunnel recognition was applied. Missing of the forward target during ACC leads to sudden acceleration, which may increase the forward collision risk. Fig. 3.7d shows the frequency response of the radar signal at the time when the target inside the iron tunnel may be missed due to a high clutter level, which is caused by the structure of the iron tunnel.

3.4 Summary

In this chapter, we have proposed a new approach that recognizes an iron tunnel using radar. Various road conditions were compared through spectrum analysis, and the features under iron-tunnel conditions were extracted. Spectrum spreading using the concept of entropy was proposed to quantitatively measure the spectral characteristics of iron tunnels. We have experimentally shown that spectrum spreading is a very useful feature for detecting iron tunnels. In addition, inside or near an iron tunnel where many clutters exist and deteriorate the target detection, iron-tunnel recognition may support ACC system to increase the performance and robustness. Although we have tested the proposed method with real field data, more field experiments may be needed

to statistically analyze the results and to find a reliable threshold for iron-tunnel recognition.

Chapter 4

Clutter Suppression

4.1 Introduction

With the grooming demand for autonomous driving, there has been paid a great attention to the incorporation of multiple sensors [2], [3]. The detection performance of the automotive radar looks outstanding compared to other sensors in poor weather conditions or poor environmental conditions of the roads. Among many applications of the automotive radar, the adaptive cruise control (ACC) and the autonomous emergency braking (AEB) using forward looking radars are the most basic functions for safety and convenience [4]–[6]. Using ACC and AEB functions, drivers can be guaranteed safety as well as convenience when visibility is poor under bad weather conditions. Nowadays, most of forward looking radars are multi-beam, multi-range (MBMR) radars which consist of integrated narrow long range beam and wide short range beam in a single radar sensor [7]. The installation rate of automotive radars worldwide will increase because of its low cost and small size by employing MBMR radar. As the signal quality of automotive radars decreases by downsizing, their detection performance should be maintained for the safety. Moreover, their detection performance

can be deteriorated by man-made structures on roads such as iron tunnels, guardrails, or soundproof walls that have high reflectivity for electromagnetic waves and generate harmonic clutters which are due to periodic structures on roads. To overcome the limitation of radar hardware, we need to implement a signal-processing technique to improve the detection performance.

There have been several studies about reflection or diffraction on road surfaces [8]–[10]. These studies have found that the detection performance of radars is dependent on the surface roughness and road slopes. Meanwhile, there have been few studies on clutters caused by man-made structures on roads [11], [12]. These studies focused on ultra wide band pulse radars, so their application to frequency-modulated continuous waves (FMCW) [13]–[15] is not appropriate. In addition, there have been several approaches to discriminate over-head or neighboring structures from stationary targets on roads [16]–[18]. A recent study has introduced a recognition method for iron tunnels that influence the detection performance of radars because of large reflections [27]. However, few of them considered the suppression method to improve the detection performance despite of clutters on roads.

In this chapter, we propose a novel harmonic clutter recognition and suppression method to overcome the deterioration of detection performance due to harmonic clutters. The proposed method recognizes harmonic clutters by analyzing the spectrum of the received signal under different road conditions. We observe that the spectrum contains equally spaced frequency peaks which are harmonic clutters due to periodic structures such as iron tunnels, guardrails, and sound-proof walls. The proposed recognition method measures the level of clutters by applying the discrete Fourier transform (DFT) to the spectrum in frequency domain and incorporating the concept of the peak-to-average-power ratio (PAPR). The proposed suppression method restrains harmonic

clutters by reducing the level of clutters. Raw experimental data were obtained using a 77-GHz forward-looking FMCW radar for the ACC and AEB. We demonstrate that the proposed method can successfully recognize and suppress harmonic clutters using real field data. In addition, the detection results show that the problem of the late detection of a target vehicle in an iron tunnel under ACC is improved by using the proposed clutter-suppression method.

This chapter is organized as follows. In Section 4.2, we present a description of the radar model and the spectral analysis of the received signal in accordance with various road environments. Then, we discuss in detail the proposed harmonic clutter-recognition method. In Section 4.3, we present and verify the proposed suppression method by performing the software-in-the-loop (SIL) test using real data obtained from the radar. In Section 4.4, we show the experimental results of the improved early detection in the ACC performance, and in 4.5, we summarize and conclude this chapter.

4.2 Clutter Recognition

In this section, we present a mathematical description of a signal model received from the radar. Then, we repeat the spectral analysis and harmonic analysis of the radar signal under various road conditions. We propose a novel method to recognize harmonic clutters based on the harmonic characteristics of periodic structures.

4.2.1 Radar Model

In this study, we employed a 77-GHz forward-looking radar of Mando Corporation using FMCW modulation. If the transmitted signal of the FMCW radar is reflected by

L targets, the discrete-time received signal can be defined as

$$\begin{aligned} x(n) &= s(n) + \nu(n) \\ &= \sum_{i=0}^{L-1} A(i)\cos(2\pi f(i)n + \phi(i)) + \nu(n) \end{aligned} \tag{4.1}$$

where $n(0 \leq n < N)$ is the discrete-time index of the received signal during a single $scan$ (which is the time unit of radar signal processing), and N is the number of samples in a single $scan$. $\nu(n)$ consists of noise components and undesired clutter signals. $A(i)$ is the amplitude of the reflected signal from each target, and $\phi(i)$ is the phase component of the received signals from each target. $f(i)$ is composed of $f_r(i)$ (which is the frequency difference due to the distance of the target and the radar) and $f_d(i)$, (which depends on the relative velocity between the radar and the target). $f_r(i)$ and $f_d(i)$ can be respectively obtained as follows

$$f_r(i) = \frac{2B}{cT} R(i) \tag{4.2}$$

and

$$f_d(i) = \frac{2f_0}{c} V_r(i) = \frac{2}{\lambda} V_r(i) \tag{4.3}$$

where B is the bandwidth, T is the duration of frequency chirping, c is the speed of light, f_0 indicates the center frequency, and $R(i)$ and $V_r(i)$ are the distance and relative velocity between the radar and each target, respectively.

Then, the frequency-domain signals that were calculated using the short-time Fourier transform (STFT) can be represented as

$$X(f, m) = STFT\big(\mathbf{x}(m)\big) \tag{4.4}$$

where f is the frequency index, m is the $scan$ index, and $\mathbf{x}(m) = [x((m-1)\cdot N), x(1+(m-1)\cdot N), ..., x(N-1+(m-1)\cdot N)]$.

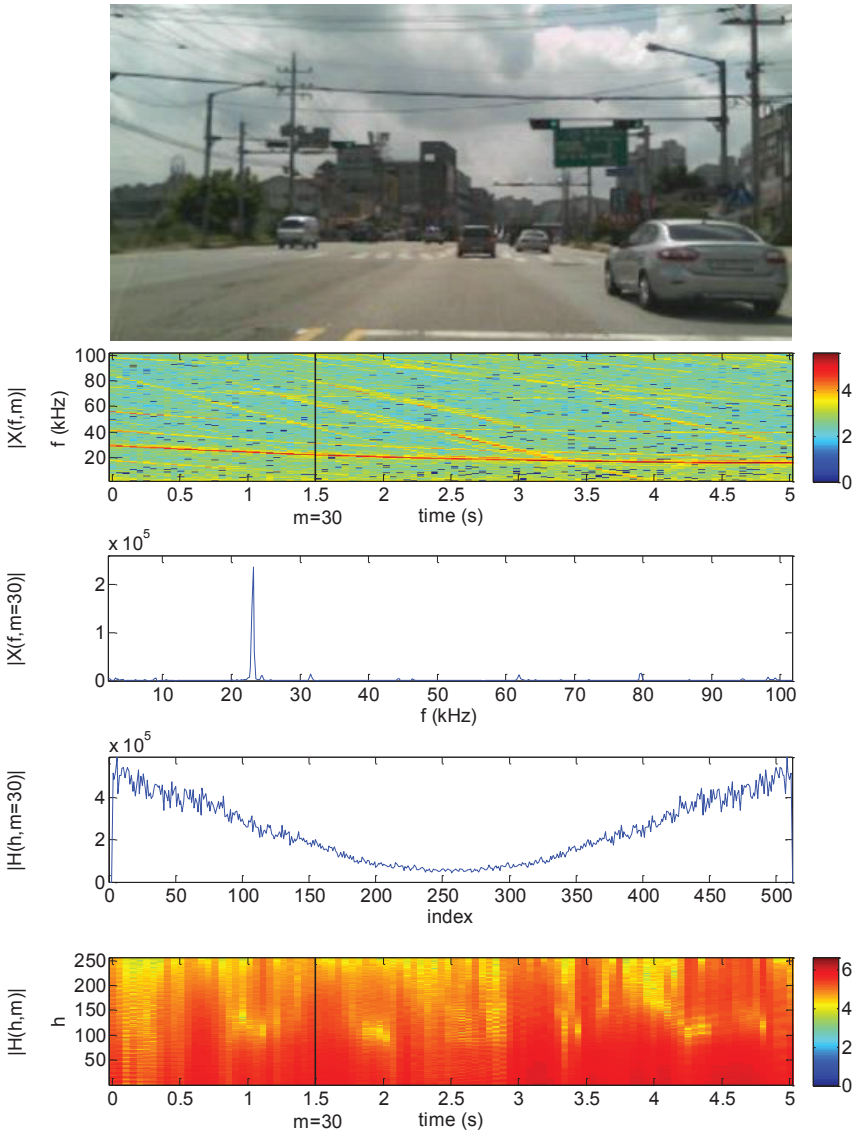

(a) Normal road

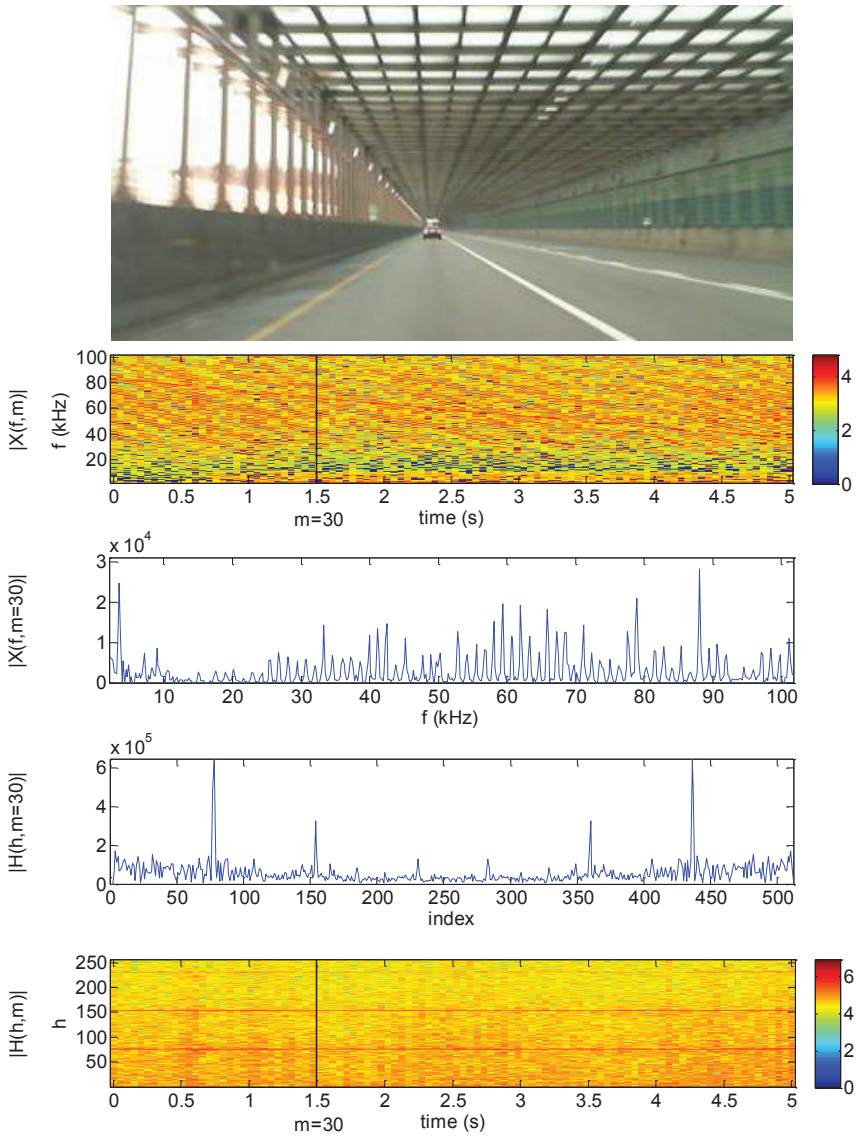

(b) Iron tunnel

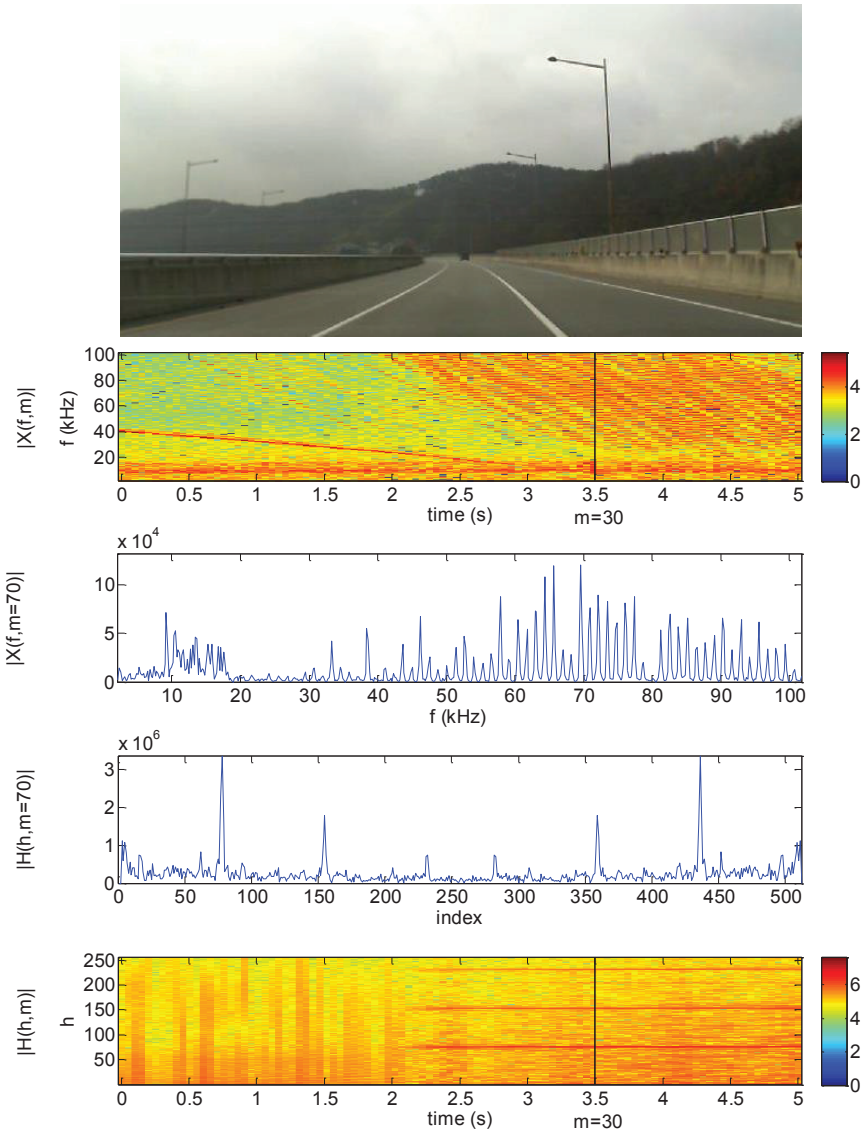

(c) Guardrail

Figure 4.1: Spectrograms and harmonograms of the received radar signal under various road conditions.

4.2.2 Spectral Analysis of Road Environment

To analyze the characteristics of the radar signal affected by clutters on the road, we compared its spectral characteristics. To extract the characteristics of clutters that adversely affect the radar, we examined the frequency characteristics using the signal acquired on a normal road, an expressway, a sound-proof wall, a guardrail, and the entry to and inside iron tunnels. In the previous study [27], we observed the spectrum spreading in dense structures such as iron tunnels, sound-proof walls, and guardrails. More interestingly, we discovered the presence of spectral harmonics in the magnitude response under such environments. To extract the harmonics, we conducted DFT on the magnitude response of the spectrum ($X(f, m)$), as follows:

$$H(h, m) = \sum_{f=0}^{N-1} \Big| X(f, m) \Big| e^{-j\frac{2\pi h}{N} \cdot f}, \tag{4.5}$$

we call $\big|H(h, m)\big|$ a *harmonogram*.

Figure 4.1 illustrates spectral harmonics under a normal road, an iron tunnel, and a guardrail. The results under each road environment consist of 5 sub-figures: the captured image on roads, the whole spectrogram, the spectrum at a certain time instance marked as the vertical solid line, the harmonogram in Equation (4.5) at the same instance in time, and the whole harmonogram.

The spectrogram ($|X(f, m)|$) in Figure 4.1a shows high intensity in the low frequency band under the normal road conditions, which indicates that a single target with a velocity that is similar to that of the own vehicle exists at the front. Other diagonal lines indicate targets have velocities that differ from that of the own vehicle, or stationary objects such as streetlights or road signs. The spectrum ($|X(f, m = 30)|$) shows the time instance ($m = 30$) marked as the vertical solid line at the spectrogram. This includes a frequency peak with high magnitude that corresponds to the target, and

low peaks from other targets. If we conduct another Fourier transform to the spectrum, we can obtain the harmonogram ($|H(h, m = 30)|$) at the same time instance in Figure 4.1a, which is symmetric because the magnitude response is real-valued. There are no notable components, and it has a flat floor. The whole harmonogram ($|H(h, m)|$) shows that there are no prominent components during the measurement time.

Figure 4.1b demonstrates the situation inside the iron tunnel. The high intensity response is spread over the entire band because of iron structures inside the tunnel in the spectrogram ($|X(f, m)|$), the spectrum ($|X(f, m = 30)|$) exhibits periodicity in the frequency-domain, and the harmonogram ($|H(f, m = 30)|$)at the time instance ($m = 30$) shows several harmonics, which represent harmonic clutters from the periodic structures. The iron tunnel consists of periodic structures that are equally spaced, so the periodic components are concentrated in harmonic peaks in the harmonogram ($|H(h, m)|$). Other signals are spread onto the floor because targets do not exist periodically like man-made structures in an iron tunnel. We confirmed that there are prominent harmonics during the measurement in the harmonogram, and these appear as horizontal lines.

Figure 4.1c shows the condition involving a guardrail on the road. The high intensity response shows up in the spectrogram ($|X(f, m)|$) as the own vehicle meets a guardrail. The frequency peaks in the spectrum ($|X(f, m = 70)|$) are densely distributed, and the harmonogram at the time instance ($m = 70$) shows prominent peaks that correspond to the periodic structures on guardrails. In the whole harmonogram, we confirmed that harmonics appear in the middle of the measurement as the own vehicle meets guardrails. Generally, iron tunnels and guardrails contain iron structures that have almost the same spacing. The peak components represent the periodic structures, which appear as harmonic clutters to the received radar signal. Many man-made

structures with high reflectivity such as iron tunnels, guardrails, and sound-proof walls consist of evenly spaced structures. Thus, if the periodicity in the spectrum can be measured, we can recognize clutters that cause harmful effects to the radar on the road.

4.2.3 Proposed Clutter-recognition Method (Measuring Harmonics of Clutter)

To recognize clutters that deteriorate the detection performance of the radar, we need a quantitative measure that can be uniformly applied. The harmonogram reveals distinct harmonic characteristics. Therefore, harmonic clutters can be recognized if we can extract the peak components from the harmonogram. Considering the peak-to-average power ratio in the harmonogram, we defined the level of harmonic clutters, L_C, using the harmonogram as follows:

$$L_C(m) = \frac{max(|H(h,m)|)^2}{|H(h,m)|^2_{mean}}. \tag{4.6}$$

We can calculate the average value, $|H(h,m)|^2_{mean}$, with the exception of peak components that designate guard cells which are adjacent cells to the peak. A majority of peak components consist of harmonic clutters, and we therefore eliminate peak components when calculating the average value to obtain a more precise value of the floor level. To verify the validity of the proposed method, we applied the proposed method to real data from a normal road, an iron tunnel, and a guardrail as shown in Figure 4.2. Figure 4.2a shows the spectrogram of the received signal and the harmonogram on a normal public road. We cannot find periodic components from the spectrogram and harmonogram, and the level of harmonic clutter, L_C, is stable with a low value. Figure 4.2b also shows the spectrogram and harmonogram at the entry

of an iron tunnel. We can confirm that horizontal lines appear around the entrance of the tunnel, which indicate the presence of harmonic clutters. The proposed level of harmonic clutters increases as the own vehicle approaches the iron tunnel. Figure 4.2c shows a similar tendency as in Figure 4.2b under the situation of a guardrail. We can confirm that the proposed method validates the stable recognition of harmonic clutters caused by periodic structures.

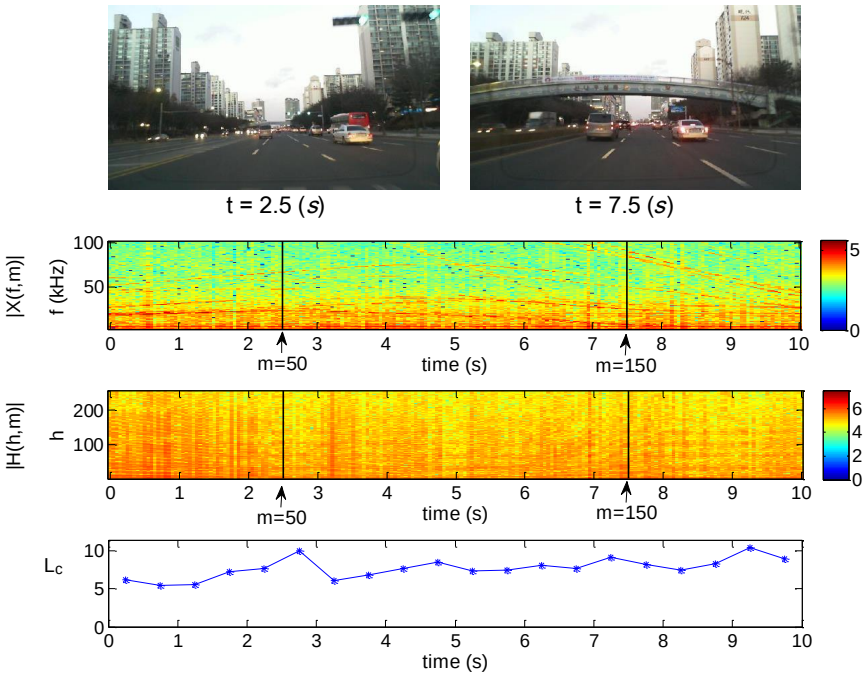

(a) Normal road

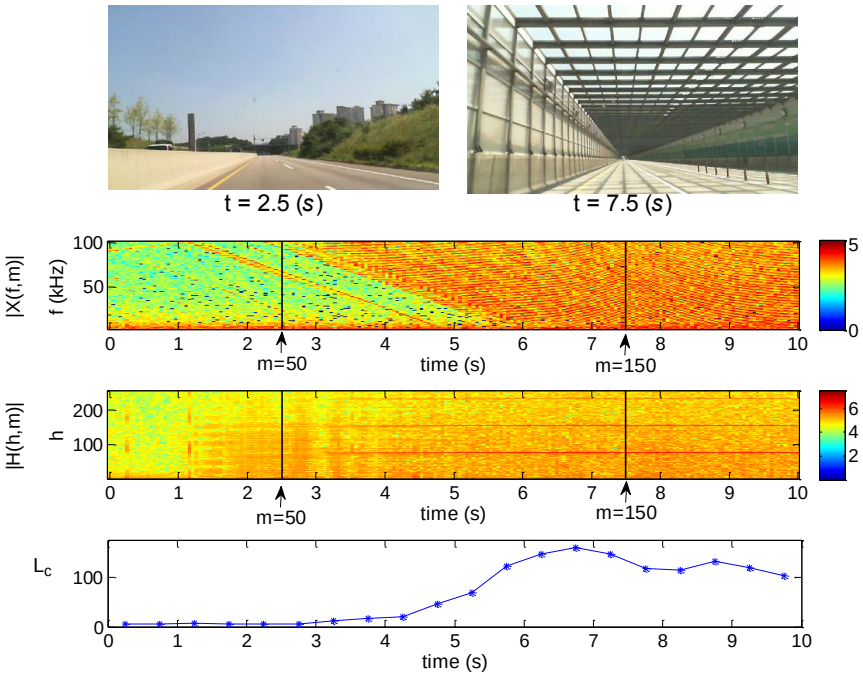

(b) Iron tunnel

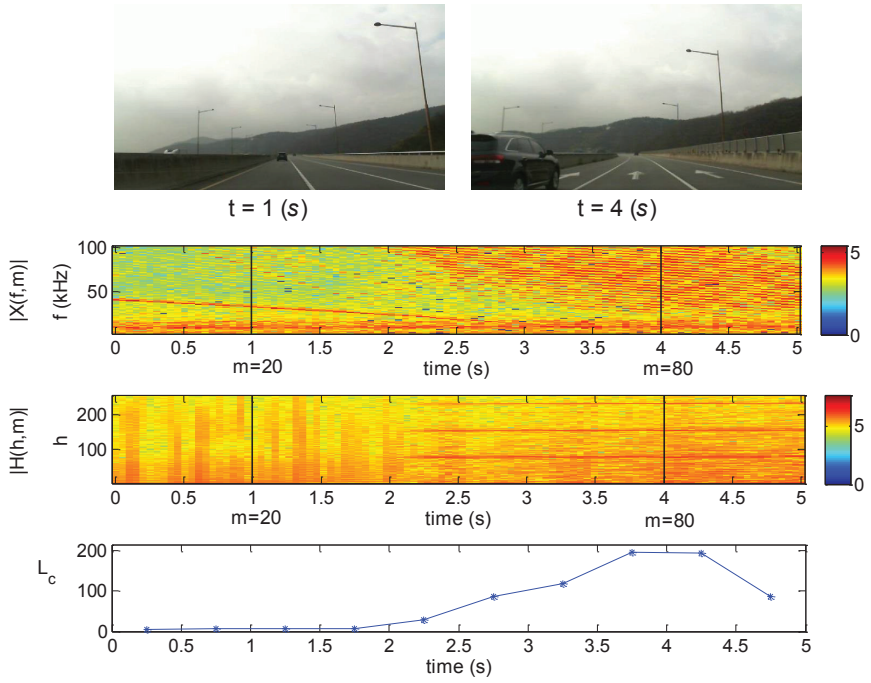

(c) Guardrail

Figure 4.2: Analysis of the level of harmonic clutter under various road conditions.

4.3 Clutter Suppression

In this section, we propose an efficient clutter-suppression method, and we evaluate the performance of the proposed method using real data acquired from the radar.

4.3.1 Proposed clutter suppression method

The conventional iron-tunnel recognition method has a limitation in terms of its ability to improve the detection performance of the radar because it controls only the parameters for signal processing, such as the threshold for extraction of target peaks or parameters of tracking algorithm. Furthermore, it does not deal with the clutter signals. In this case, there is an increased probability of occurring false alarm. Thus, it can increase the signal processing required after frequency-peak extraction, including the tracking algorithm to prevent false alarm.

To reduce this risk, we propose a new approach to suppress harmonic clutters maintaining signals from targets. If harmonic clutters can be recognized using the proposed method, we can reduce clutters by suppressing the peak components of the magnitude response from the DFT ($|H(h,m)|$). Harmonic peaks contain concentrated clutter signals and spread target signals. The loss of information from targets is negligible because the components of clutter signals are much higher than those of target signals. We can extract the harmonic peaks in the magnitude response of $|H(h,m)|$ by simply using the cell-averaging constant false alarm rate (CA-CFAR) algorithm [26].

If the presence of clutters is recognized from the recognition method, we calculate the average value of the magnitude of reference cells which are included in a window under the test around each peak from the CA-CFAR algorithm, with the exception of guard cells. Then, we set the magnitude value of guard cells, including the peak cell,

as the average of the reference cells maintaining the phase of each cell as follows:

$$\overline{H(h,m)} = \begin{cases} A_r(k)e^{j\phi(h)},\ h_{p(k)} - \frac{N_g}{2} \leq h \leq h_{p(k)} + \frac{N_g}{2} \text{ if } L_C(m) > L_{th} \\ H(h,m) \quad ,\ \text{otherwise} \end{cases} \tag{4.7}$$

where $\overline{H(h,m)}$ is the harmonic clutter suppressed harmonogram, $A_r(k)$ is the average magnitude of reference cells, $\phi(h)$ is the phase component of $H(h,m)$, $h_{p(k)}$ represents the index of the kth peak, N_g is the number of guard cells, and L_{th} is the threshold of the level of harmonic clutter for recognition which is calculated as 3 times of mean power of harmonogram at normal road condition. To better understand the usefulness of the proposed method, we conducted harmonic clutter suppression using data obtained in an iron tunnel at an instance in time when the target was not extracted as in Figure 4.3. The first figure is the spectrogram, and the vertical solid line indicates the instance in time, which we investigated to compare the effect of the proposed clutter-suppression method. The next figure is the spectrum of the received signal in an iron tunnel, where there is a target vehicle in front of the own vehicle. The next figure shows the harmonogram in the same time instance of the spectrum. We can confirm that several peaks from harmonic clutters, which are due to periodic structures, and the rest of the signal floor are as a result of the targets. The clutters appear as periodic signals, so the clutters are compressed by the DFT, and concentrated into harmonic peaks. The fourth figure represents the whole harmonogram, and the next figure is the harmonic clutter suppressed harmonogram ($|\overline{H(h,m)}|$). The dashed line in the sixth figure represents the suppressed harmonogram in a certain time instance ($|\overline{H(h,m=123)}|$). The next figure is the harmonic clutter-suppressed spectrum which denotes the magnitude of the result of inverse DFT (IDFT) of the previous peak-suppressed signal. Although

the entire signal level is reduced, the decrease in the signal from the target is negligible because the majority of the suppressed peaks are from harmonic clutters. We can confirm that the signal from the target vehicle is obtained by conventional signal processing algorithm. The final figure indicates the harmonic clutter suppressed spectrogram ($|\overline{X(f,m)}|$). The overall intensity is decreased, and the diagonal lines in the spectrum are particularly suppressed.

4.3.2 Verification using real data

To verify that harmonic clutters can be recognized and suppressed using the proposed method, we tested the proposed method using acquired data in various road environments that contain harmonic clutters. Table 4.1 summarizes the types of harmonic clutters for which we conducted experiments, the dates of the experiment, the latitudinal and longitudinal coordinates of the clutters, the entry time and exit time, the average level of clutters in dB scale where there are harmonic clutters without and with clutter suppression, and the clutter-suppression ratio (CSR) by calculating the difference of average level of clutters according to suppression as

$$CSR = \frac{10\log_{10}(L_{c,without}) - 10\log_{10}(L_{c,with})}{10\log_{10}(L_{c,without})} \times 100 \tag{4.8}$$

where $L_{c,without}$ and $L_{c,with}$ represent the average value of the level of clutters without and with suppression, respectively. The types of harmonic cutters contain an iron-tunnel (IT), a guardrail (GR), and a sound-proof wall (SP).

We confirmed that there are significant differences between the average values of the level of harmonic clutters, L_C, without and with the clutter suppression. Figure 4.4a shows the effect of clutter suppression around the exit point of an iron-tunnel. The first figure is the spectrogram of the received signal. The second and third fig-

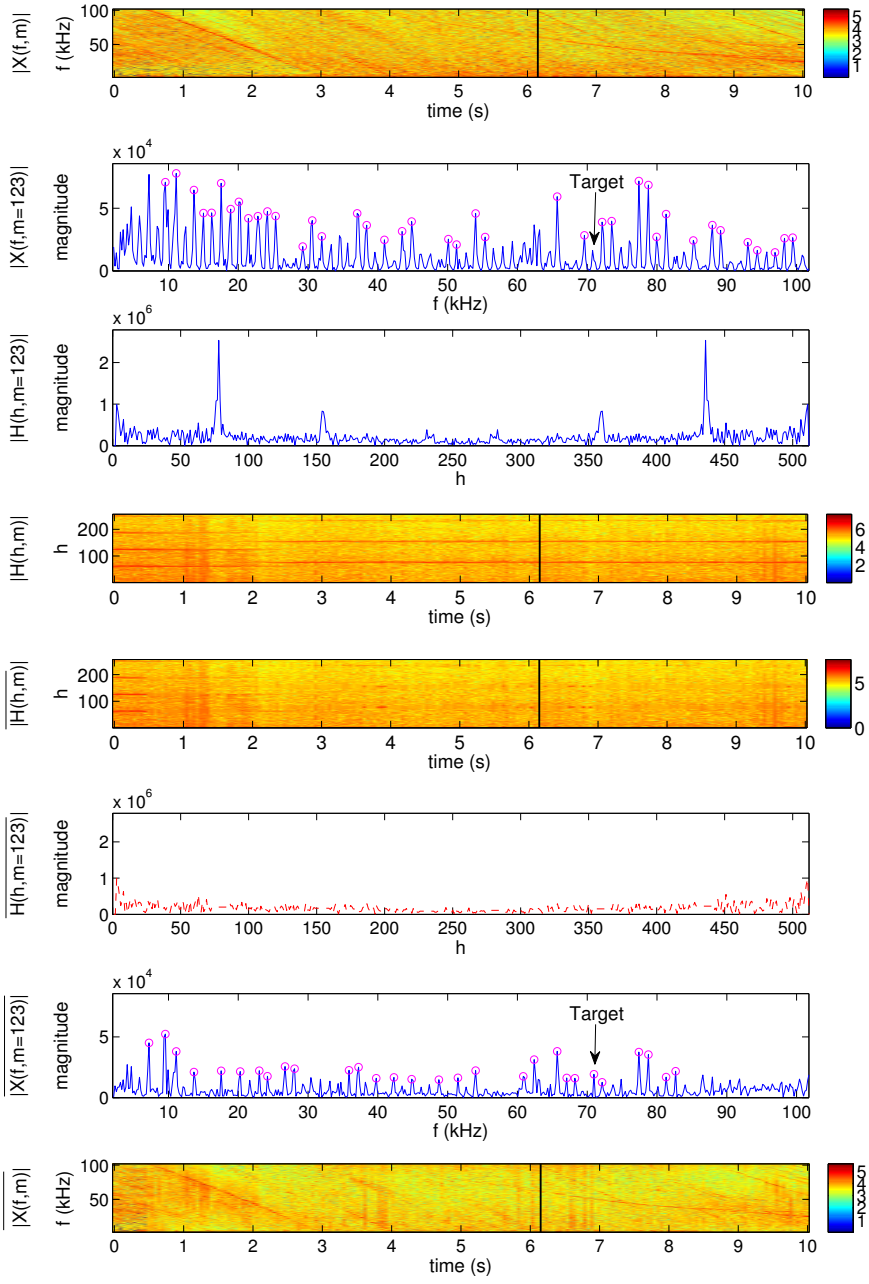

Figure 4.3: An example of clutter suppression results in an iron tunnel.

Table 4.1: Profile of various harmonic clutters and the level of harmonic clutter

Case	Type	Date of Experiment	Geographic coordinate (latitude, longitude)	Time (s)		$10\log_{10}(P_c)$ (dB)		CSR(%)
				Entry	Exit	without	with	
A	IT	Nov.16.15	(32.27, 127.08)	-	4.75	20.79	4.69	77.4
B	IT	Aug.18.15	(32.17, 127.03)	5.75	-	21.08	4.74	77.5
C	IT	Aug.11.15	(32.27, 127.08)	6.25	17.75	19.35	4.94	77.5
D	IT	Jan.02.16	(36.47, 127.25)	10.75	-	20.36	4.59	77.5
E	IT	Jan.02.16	(36.47, 127.25)	-	15.25	19.49	5.19	73.4
F	IT	Aug.13.15	(32.17, 127.03)	3.25	-	21.16	4.71	77.7
G	GR	Nov.20.15	(32.27, 127.08)	3.25	-	21.71	4.89	77.5
H	GR	Aug.18.15	(32.27, 127.08)	6.25	-	13.73	5.12	62.7
I	SP	Nov.16.15	(32.27, 127.08)	5.25	-	19.96	4.94	75.3

ures represent the harmonogram containing clear horizontal lines, which are due to concentrated harmonic clutters, and the level of harmonic clutters, which has a high value before the exit point. The fourth and fifth figures show the harmonogram and the level of harmonic clutters after harmonic clutter suppression. We confirmed that horizontal lines are removed after the suppression, and the level of clutters remains stable from the beginning to the end of data. The final figure represents the harmonic clutter suppressed spectrogram.

Figure 4.4b shows the location around the entry point of an iron tunnel. Similarly, we observe horizontal lines in the second figure, and a high L_C after the entry point without the suppression. The harmonic clutter suppressed harmonogram ($\overline{H(h,m)}$), L_C, and the harmonic clutter-suppressed spectrum ($\overline{X(f,m)}$) indicate the effect of the proposed harmonic clutter- suppression method clearly.

Figure 4.4c shows a similar tendency as Figure 4.4b around a guardrail on the curved road. The intensity at high frequency is stronger than low frequency, because the reflected signals from close guardrails laid on the edge of roads are weak. However, reflected signals from long distances can be strong enough to disrupt the signals from a target in front of the own vehicle. Moreover, the probabilities of those effects can be increased on curved roads because reflections are higher than on the straight roads. The results obtained for harmonic clutter suppression are similar to those of previous cases.

4.4 Experimental results

To determine the usefulness of the proposed harmonic clutter-suppression method for ACC, we performed an experiment without the proposed method, and we gathered

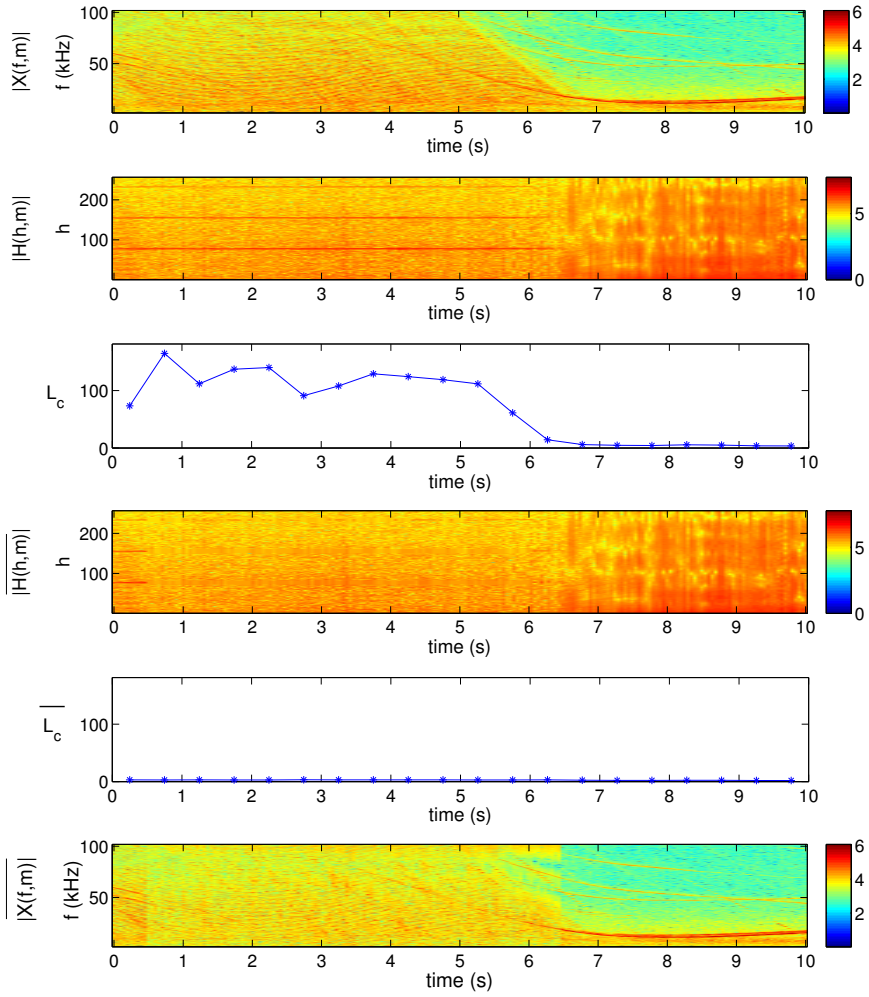

(a) Case A (CSR = 77.4%)

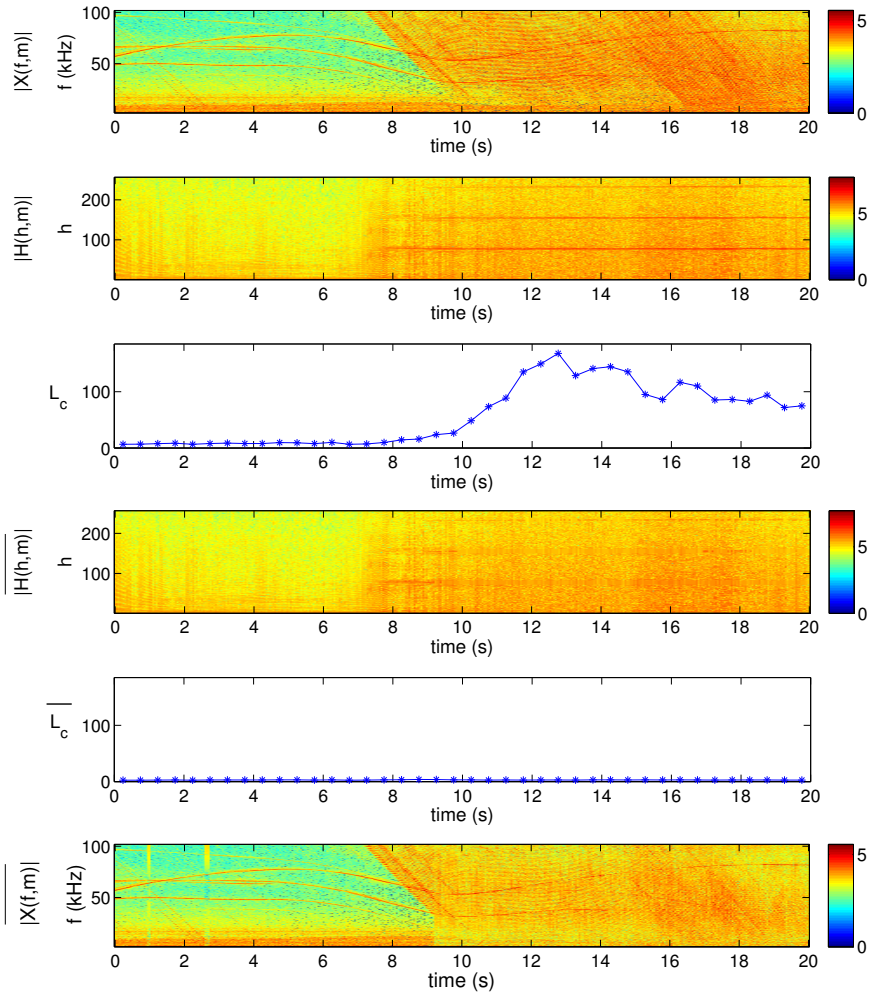

(b) Case D (CSR = 77.5%)

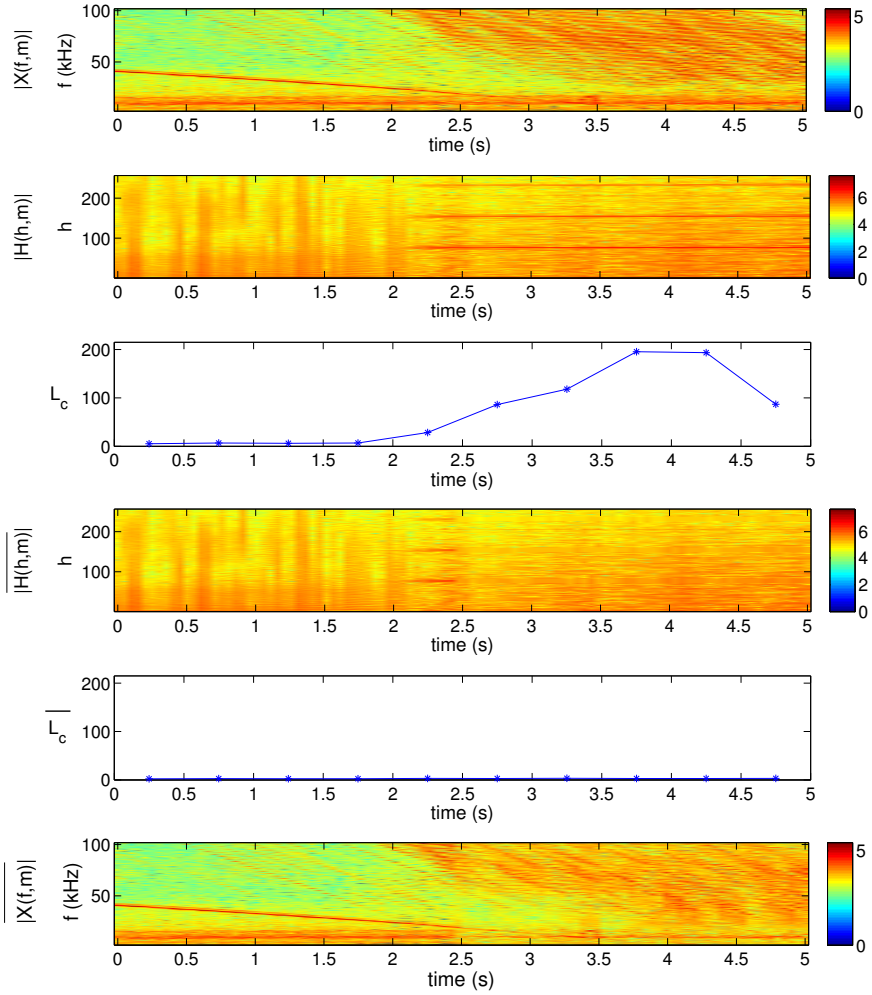

(c) Case G (CSR = 77.5%)

Figure 4.4: Results of harmonic clutter suppression.

raw data from the radar. The bandwidth (B) of the transmitted signal is 500 MHz and the chirp duration (T) is 5 ms with the center frequency (f_c) at 76.5 GHz. We conducted an SIL test using the same data to compare how quickly targets or vehicles are detected in the lane of the own vehicle with and without the proposed method inside an iron tunnel. We set the vehicle speed to ACC = 180 kph, and the own vehicle was accelerated because of the absence of a target vehicle in the maximum detection range at the front. Then, the accelerating own vehicle performed sudden deceleration because of the late detection of the target vehicle. This situation could be dangerous if the distance between the own vehicle and the following vehicle is close.

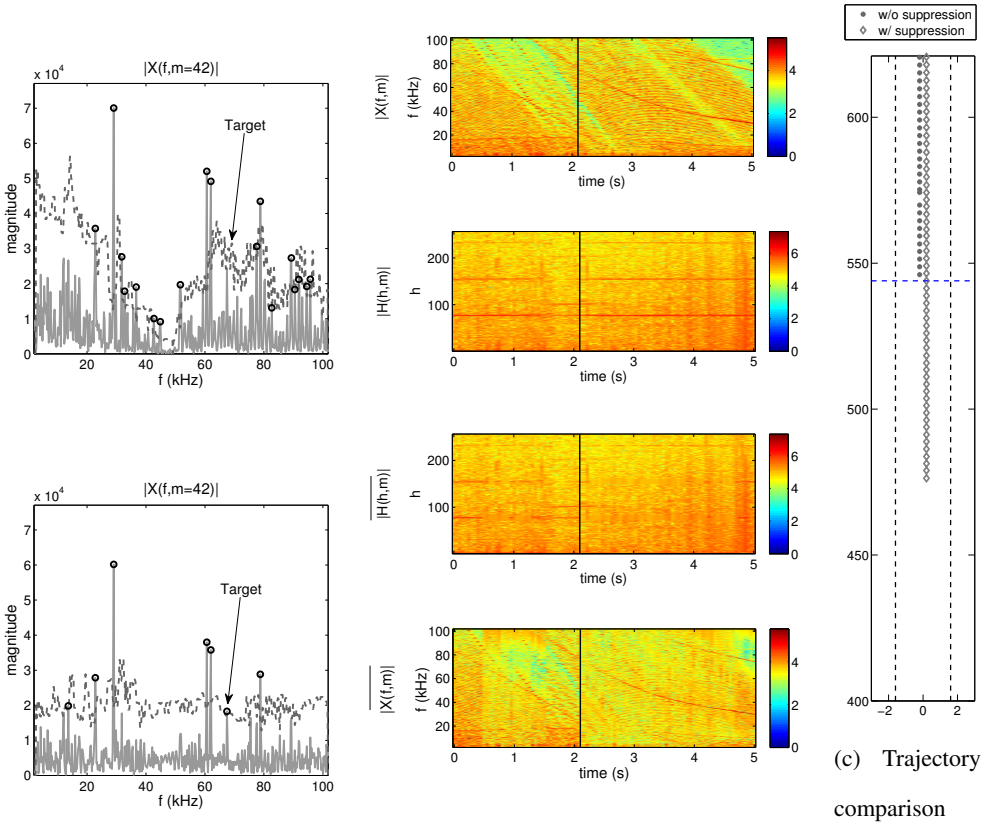

(a) Spectrum comparison.

(b) Comparison of spectrogram and harmonogram.

(c) Trajectory comparison of detection result.

Figure 4.5: Comparison of detection result (Early detection).

Figure 4.5 shows the detection results with and without application of the harmonic clutter-suppression method during the detection of the forward target vehicle inside the iron tunnel. Figure 4.5a show the spectrum comparison at the instance of time just before the target vehicle is detected by the radar of the own vehicle, and this is represented as the horizontal dashed line in Figure 4.5c. The first spectrum represents the original spectrum obtained in the field experiment. There are many high-intensity harmonic clutters, so the target vehicle cannot be extracted because of the high clutter level. We confirmed that the spectrum after harmonic clutter suppression contains fewer clutter signals, whereas remaining information of targets. The frequency peak of the vehicle in front of the own vehicle can be obtained using the conventional CFAR algorithm.

Figure 4.5b show spectrograms and harmonograms without and with the proposed method respectively. The spectrogram and harmonogram without clutter suppression contain many clutter signals. On the other hand, we can confirm that horizontal lines by harmonic peaks are removed in the harmonogram and diagonal lines with high intensity in the spectrogram are eliminated when we apply the proposed method.

Figure 4.5c shows the trajectory of the detected target vehicle along the distance axis. We can confirm that when harmonic clutters are suppressed using the proposed method, the target vehicle can be detected at an earlier time. The initial detection time is a critical factor in determining the performance of the ACC. The speed of the own vehicle was 170.6 kph because of the continuous acceleration until the detection of the target vehicle in front of it, and the distance between the target vehicle and the own vehicle was 104.1 m when the target vehicle was initially detected. The driver in the own vehicle had to made a sudden deceleration to avoid a collision. However, the distance between the target vehicle and the own vehicle was 169.85 m after harmonic-

clutter suppression. In this case, there is no need to make an abrupt deceleration, and there was sufficient time to comfortably control the own vehicle.

4.5 Summary

In this chapter, we proposed new approaches for the detection and suppression of harmonic clutters on roads using an automotive radar. We performed spectral and harmonic analyses of the radar signal received in various road conditions using a conventional spectrogram and suggested harmonogram. We then obtained the features under harmonic clutters using those analysis results. We proposed a level of harmonic clutters using the PAPR concept with a harmonogram to measure the characteristics of harmonic clutters quantitatively. We also proposed the suppression method of harmonic clutters by reducing the level of clutters of the spectrum. We performed experiments to verify that the proposed level of the clutter-based method is very useful for recognizing and suppressing harmonic clutters. In addition, the proposed harmonic clutter recognition and suppression method improved the performance and robustness of an ACC system where there were severe harmonic clutters which reduced detection performance of the radar. Although we performed the proposed method using several sets of real data acquired from public roads, more field tests may be needed to enable a statistical analysis of the proposed methods.

Chapter 5

Conclusion and Future Works

In this dissertation, we have proposed an advanced multi-beam and multi-range automotive radar for ACC and AEB. Based on the theoretical background, system parameters were designed to fulfill the system requirement, and an efficient hardware structure was proposed for the actual implementation. The signal processing structures optimized for the proposed hardware were designed and implemented as an embedded software. Advanced modulation and signal processing scheme are proposed to satisfy the requirements for AEB scenario. In order to verify the detection performance of the radar, basic tests are performed in RF anechoic chamber using RTS. The detection results of range, velocity, and angle information were properly extracted from the radar. To confirm the detection coverage performance, we performed field test in the open space using test vehicle. The detection result have satisfied with the system requirement.

To overcome detection problem from field test for design validation, we have proposed a new approach that recognizes an iron tunnel using radar. Various road conditions were compared through spectrum analysis, and the features under iron-tunnel

conditions were extracted. Spectrum spreading using the concept of entropy was proposed to quantitatively measure the spectral characteristics of iron tunnels. We have experimentally shown that spectrum spreading is a very useful feature for detecting iron tunnels. In addition, inside or near an iron tunnel where many clutters exist and deteriorate the target detection, iron-tunnel recognition may support ACC system to increase the performance and robustness.

To expand a range of application, we proposed new approaches for the recognition and suppression of harmonic clutters on roads using an automotive radar. We performed spectral and harmonic analyses of the radar signal received in various road conditions using a conventional spectrogram and suggested harmonogram. We then obtained the features under harmonic clutters using those analysis results. We proposed a level of harmonic clutters using the PAPR concept with a harmonogram to measure the characteristics of harmonic clutters quantitatively. We also proposed the suppression method of harmonic clutters by reducing the level of clutters of the spectrum. We performed experiments to verify that the proposed level of the clutter-based method is very useful for recognizing and suppressing harmonic clutters. In addition, the proposed harmonic clutter recognition and suppression method improved the performance and robustness of an ACC system where there were severe harmonic clutters which reduced detection performance of the radar.

The proposed signal processing schemes for recognition of environments using automotive radar are novel attempts without two dimensional image information. Although we performed the proposed method using several sets of real data acquired from public roads, more field tests may be needed to enable a statistical analysis of the proposed methods. The author is interested in advanced modulation sheme beyound FMCW such as fast-chirp and code division for MIMO radar. The proposed environ-

ment recognition method can be improved with fast-chirp modulation containng more information and the range of recognition can be expanded to other objects such as vehicles, pedesrians, and various road structures. Advanced target recognition technique can be realized by machine learning algorithms including deep learing.

Bibliography

[1] World Health Organization, *Global status report on road safety 2015.*

[2] R. Okuda, Y. Kajiwara, and K. Terashima, "A survey of technical trend of ADAS and autonomous driving," *VLSI Technology, Systems and Application (VLSI-TSA), Proceedings of Technical Program - International Symposium on*, pp. 1–4, Apr. 2014.

[3] Dickmann, J., Klappstein, J., Hahn, M., Appenrodt, N., Bloecher, H., Werber, K., Sailer, A.: 'Automotive Radar the Key Technology For Autonomous Driving: From Detection and Ranging to Environmental Understanding,' *2016 IEEE Radar Conf.*, pp. 1–6, Apr. 2016.

[4] E. Coelingh, A. Eidehall and M. Bengtsson, "Collision Warning with Full Auto Brake and Pedestrian Detection - a practical example of Automatic Emergency Braking," *13th International IEEE Conference on Intelligent Transportation Systems*, pp. 155–160, Sep. 2010.

[5] H. Kopetz, and S. Poledna, "Autonomous Emergency Braking: A System-of-Systems perspective,," *Dependable Systems and Networks Workshop (DSN-W), 2013 43rd Annual IEEE/IFIP Conference on*, pp. 1–7, June 2013.

[6] A. Vahidi, and A. Eskandarian, "Research advances in intelligent collision avoidance and adaptive cruise control," *IEEE Trans. Intell. Transp. Syst.*, vol. 4, no. 3, pp. 143–153, Sep. 2003.

[7] Jeong, S. H., Yu, H. Y., Lee, J. E., Oh, J. N.: 'A Multi-Beam and Multi-Range Radar with FMCW and Digital Beam Forming for Automotive Applications,' *Prog. In Electromagn. Res.*, vol. 124, pp. 285-–299, 2012.

[8] L. L. Nagy, "Electromagnetic Reflectivity Characteristics of Road Surfaces," *IEEE Trans. Vehicular Technology*, vol. 23, no. 4, pp. 117–124, Jul. 1974.

[9] R. Schneider, D. Didascalou, and W. Wiesbeck, "Impact of Road Surfaces on Millimeter-Wave Propagation," *IEEE Trans. Vehicular Technology*, vol. 49, no. 4, pp. 1314–1320, Jul. 2000.

[10] P. H. Pathak, W. D. Burnside, and R. J. Marhefka, "A uniform GTD analysis of the diffraction of electromagnetic waves by a smooth convex surface," *IEEE Trans. Antenna and Propagation*, vol. AP-28, no. 5, pp. 631–642, Sep. 1980.

[11] C. Bouvier, L. Martinet, G. Favier, H. Sedano, and M. Artaud, "Radar clutter classification using autoregressive modeling, K-distribution and neural network," *IEEE International Conference on Acoustics, Speech, and Signal Processing*, vol. 3, pp. 1820–1823, May. 1995.

[12] I. Matsunami, and A. Kajiwara, "Clutter suppression scheme for vehicle radar," *IEEE Radio and Wireless Symposium*, pp. 320–323, Jan. 2010.

[13] A. G. Stove, "Linear FMCW radar techniques," *IEE Proceedings-F*, vol. 139, no. 5, Oct. 1992.

[14] M. I. Skolnik, *Introduction to Radar Systems*, New York, McGraw-Hill Book Company, 2001.

[15] D. K. Barton, *Radar System Analysis and Modeling*, Norwood, MA, Artech House, 2004.

[16] C. Lundquist, and T. B. Schön, "Tracking stationary extended objects for road mapping using radar measurements," *IEEE Inteligent Vehicles Symp.*, pp. 405–410, Jun. 2009.

[17] F. Diewald, J. Klappstein, F. Sarholz, J. Dickmann, K. Dietmayer, "Radar-interference-based bridge identification for collision avoidance systems," *IEEE Intelligent Vehicles Symposium*, pp. 113–118, Jun. 2011.

[18] K. R. Choi, G. H. Seo, J. E. Lee,S. H. Jeong, and J. N. Oh, "Automatic radar horizontal alignment scheme using stationary target on public Road," *Radar Conference (EuRAD)*, pp. 551–554, Oct. 2013.

[19] EU Regulation No. 347/2012

[20] Tokoro, S., K. Kuroda, and A. Kawakubo, "Automotive electronically scanned millimeter-wave radar," *SICE Annual Conference*, 42–47, Fukui, August 4–6, 2003.

[21] D. Freundt and B. Lucas, "Long range radar sensor for high-volume driver assistance systems market," *SAE World Congress & Exhibition*, 2008.

[22] Z. Chen, and S. Otto, "A taper optimization for pattern synthesis of microstrip series-fed patch array antennas," *IEEE EUWIT*, 160–163, 2009.

[23] C. A. Balanis, *Antenna Theory: Analysis and Design*, Wiley, 2007.

[24] B. R. Mahafza, *Radar System Analysis and Design using Matlab*, Boca Raton, FL: CRC, 2000.

[25] H. Krim and M. Viberg, 'Two decades of array signal processing research," *IEEE Signal Processing Magazine*, vol. 13, no. 4, pp. 67–94, Jul. 1996.

[26] H. Rohling, "Radar CFAR thresholding in clutter and multiple target situations," *IEEE Trans. Aerospace and Electronic Systems*, vol. AES-19, no. 4, pp. 608–621, Jul. 1983.

[27] J. E. Lee, H. S. Lem, S. H. Jeong, S. C. Kim, and H. C. Shin, "Enhanced iron-tunnel recognition for automotive radars," *IEEE Trans. Vehicular Technoloy*, vol. 65, no. 6, pp. 4412–4418, Jun. 2016.

초 록

도로 상의 차량의 수가 점차 증가하면서 교통사고 및 교통사고 사망자의 수 역시 점차 증가하고 있다. 대부분의 사고는 운전자의 부주의로 인해 발생하기 때문에 운전자를 보조하기 위한 운전자 보조 시스템(DAS)에 대한 관심이 증가하고 있고 다양한 DAS 센서들 중에서 레이더는 악천후나 도로 환경에 영향을 적게 받기 때문에 카메라나 라이다(Lidar)와 같은 센서들에 비해 안정적인 성능을 가지고 있다. 차량용 레이더를 이용한 애플리케이션은 다양한데 이 중에서 적응 순항 제어 (Adaptive Cruise Control)과 자동 긴급 제동 (Autonomous Emergency Braking)이 가장 대표적인 기능이다. 이전에는 이러한 ACC와 AEB를 위한 전방 레이더는 장거리용 레이더 하나와 근거리용 레이더 두개로 구성되어 시스템 비용이 굉장히 높았다. AEB등의 기능이 안전을 위해 표준화 되고 있고 점차 자율주행에 대한 관심이 높아지면서 차량용 레이더의 장착율이 높아지고 있고 더욱 확대될 것으로 전망된다. 따라서 레이더 시스템의 가격을 낮출 필요성이 생겨나고 이와 함께 집적화된 반도체 기술이 발전하여 레이더 개발 업체의 차량용 레이더 가격 경쟁이 점점 치열해지고 있다.

본 논문에서는 ACC와 AEB 기능을 위한 다중 빔 다중 범위 차량용 전방 레이더를 설계 및 제작하고 성능을 검증한다. 장거리 감지 레이더와 근거리 감지 레이더를 통합 함으로써 레이더 센서의 사이즈를 축소시키고 가격을 낮춤으로

써 레이더 장착의 대중화에 기여할 수 있는 고성능 레이더를 제안한다. 안테나 배열을 포함한 효율적인 하드웨어 구조 및 최적화된 신호처리 구조를 제시하며 실제 제작된 레이더를 이용하여 검증 실험을 진행하여 제안하는 레이더의 성능을 확인할 수 있다.

또한 차량용 레이더에서는 불가능하다고 여겨진 환경 인식 기술을 제시한다. 일반적인 도로가 아닌 철제 터널과 같이 구조물이 조밀하게 설치되어 있는 경우 레이더에서 송신하는 신호가 반사되어 수신 되는 클러터 (Clutter) 신호가 많은데 이러한 경우 실제 타겟 차량에서 수신되는 신호보다 강도가 센 경우가 있고 이로 인해 감지의 안정성이 열화 될 수 있다. 본 논문에서는 이러한 철제터널 환경을 수신 신호를 분석하여 인식하는 방법을 제시하고 제안하는 실제 레이더를 이용하여 도로 주행 시험을 수행하여 제안하는 방법의 실효성을 검증한다.

철제터널 이외에도 도로상의 가드레일이나 방음벽과 같이 클러터 신호를 많이 발생 시키는 구조물에 대한 연구로 확장하여 이러한 인공적인 구조물은 일정한 간격으로 구조물이 배치되어 있기 때문에 수신 신호의 주파수 도메인 상의 스펙트럼에 클러터 신호가 주기적으로 나타나게 되고 이러한 주기적 신호의 정도를 측정할 수 있는 방법을 제시한다. 주기성을 가지는 클러터를 인식한 경우 클러터 신호를 억제함으로써 타겟으로부터 수신한 신호의 품질을 향상 시키고 레이더의 감지 성능을 높일 수 있는 방법을 함께 제시한다. 이러한 방법을 검증하기 위해 도로 상의 철제터널, 가드레일, 방음벽을 대상으로 실제 주행 시험을 실시하여 제안하는 방법을 검증하였고 이를 통해 레이더 감지 성능이 향상됨을 확인할 수 있다.

본 논문에서 사용한 데이터는 모두 챕터2에서 제안하는 (주)만도의 77GHz 대역의 전방 레이더를 사용하였다. 레이더 데이터를 이용하여 도로 상황에 대한 주파수 분석을 하였으며 제안하는 철제터널 및 구조물 인식 결과와 클러터 억제에 대한 유효성 검증 또한 실제 데이터를 통해 확인하였다.

주요어: 차량용 레이더, MBMR, Clutter Recognition, Clutter Suppression

학번: 2013-30251